Draft version January 24, 2018
Typeset using LaTeX **preprint2** style in AASTeX61

DISCOVERY OF A TRANSITING ADOLESCENT SUB-NEPTUNE EXOPLANET IN THE CAS-TAU ASSOCIATION WITH K2

Trevor J. David,[1] Eric E. Mamajek,[1,2] Andrew Vanderburg,[3,*] Joshua E. Schlieder,[4]
Makennah Bristow,[5] Erik A. Petigura,[6,†] David R. Ciardi,[7] Ian J. M. Crossfield,[8]
Howard T. Isaacson,[9] Ann Marie Cody,[10] John R. Stauffer,[11] Lynne A. Hillenbrand,[6]
Allyson Bieryla,[12] David W. Latham,[12] Benjamin J. Fulton,[6] Luisa M. Rebull,[13,11]
Chas Beichman,[14] Erica J. Gonzales,[15,‡] Lea A. Hirsch,[9] Andrew W. Howard,[6]
Gautam Vasisht,[1] and Marie Ygouf[16]

[1] *Jet Propulsion Laboratory, California Institute of Technology, 4800 Oak Grove Drive, Pasadena, CA 91109, USA*
[2] *Department of Physics & Astronomy, University of Rochester, Rochester, NY 14627, USA*
[3] *Department of Astronomy, The University of Texas at Austin, Austin, TX 78712, USA*
[4] *Exoplanets and Stellar Astrophysics Laboratory, Code 667, NASA Goddard Space Flight Center, Greenbelt, MD 20771, USA*
[5] *Department of Physics, University of North Carolina at Asheville, Asheville, NC 28804, USA*
[6] *Department of Astronomy, California Institute of Technology, Pasadena, CA 91125, USA*
[7] *Caltech/IPAC-NASA Exoplanet Science Institute, Pasadena, CA 91125, USA*
[8] *Department of Physics, Massachusetts Institute of Technology, Cambridge, MA, USA*
[9] *Astronomy Department, University of California, Berkeley, CA 94720, USA*
[10] *NASA Ames Research Center, Moffet Field, CA 94035, USA*
[11] *Spitzer Science Center (SSC), Infrared Processing and Analysis Center (IPAC), California Institute of Technology, Pasadena, CA 91125, USA*
[12] *Harvard–Smithsonian Center for Astrophysics, Cambridge, MA 02138, USA*
[13] *Infrared Science Archive (IRSA), Infrared Processing and Analysis Center (IPAC), California Institute of Technology, Pasadena, CA 91125, USA*
[14] *NASA Exoplanet Science Institute, California Institute of Technology, Jet Propulsion Laboratory, Pasadena, CA 91125, USA*
[15] *Astronomy and Astrophysics Department, University of California, Santa Cruz, CA, USA*
[16] *Infrared Processing and Analysis Center (IPAC), California Institute of Technology, Pasadena, CA 91125, USA*

(Received; Revised; Accepted)

Submitted to AAS Journals

ABSTRACT

The role of stellar age in the measured properties and occurrence rates of exoplanets is not well understood. This is in part due to a paucity of young planets and the uncertainties in age-dating for most exoplanet host stars. Exoplanets belonging to coeval stellar populations, young or old, are particularly useful as benchmarks for studies aiming to constrain the evolutionary timescales relevant for planets. Such timescales may concern orbital migration, gravitational contraction, or atmospheric photo-evaporation, among other mechanisms. Here we report the serendipitous discovery

Corresponding author: Trevor J. David
trevor.j.david@jpl.nasa.gov

of a transiting sub-Neptune from *K2* photometry of the low-mass star EPIC 247267267. From multiple age indicators we estimate the age of the star to be in the range of 50–500 Myr at 68% confidence. However, based on its kinematics, we propose the star belongs to the Cas-Tau association, which we suggest has an age of 46 $\pm$ 8 Myr. Our newly derived age estimate for the association is based on a color-magnitude diagram analysis of high-probability members near the main sequence turnoff. The size of EPIC 247267267 b (R_P = 3.0 $\pm$ 0.5 $R_\oplus$) combined with its youth make it an intriguing case study for photo-evaporation models, which predict enhanced atmospheric mass loss during early evolutionary stages.

Keywords: planets and satellites: physical evolution — planets and satellites: gaseous planets — stars: low-mass — stars: planetary systems — Galaxy: open clusters and associations: individual (Cas-Tau)

* NASA Sagan Fellow
† NASA Hubble Fellow
‡ NSF Graduate Research Fellow

1. INTRODUCTION

Exoplanet properties are intrinsically linked to the properties of their host stars. The primary parameters governing stellar structure are mass, metallicity, and age. Planet occurrence is known to correlate with stellar mass (Cumming et al. 2008; Howard et al. 2012) and metallicity (Fischer & Valenti 2005). The degree to which planet demographics are time-dependent, however, remains under-explored. This is due to both the scarcity of young planets as well as the large uncertainties in the ages of typical exoplanet hosts. Compiling a sample of planetary systems with well-constrained ages is a critical step on the path towards statistical comparisons of the frequencies and properties of planets across time.

There is a long history of planet searches within clusters and other coeval stellar populations. Early wide-field transit searches for hot Jupiters targeted globular clusters for the large sample sizes afforded by these populations (Gilliland et al. 2000; Weldrake et al. 2005, 2008). These searches resulted in no detections, leading to a claim of lower occurrence rates within older populations. However, Masuda & Winn (2017) revisited that claim and concluded the globular cluster null results were consistent with *Kepler* hot Jupiter statistics after accounting for frequency trends with stellar mass.

Within open clusters of intermediate (∼1–7 Gyr) and young ages (<1 Gyr), numerous surveys have searched for planets across a wide range of mass and separation, using the transit, radial velocity (RV) and direct imaging methods (see Bowler 2016, for a review of young exoplanets detected through imaging). In the ∼3.5 Gyr-old M67 cluster, there is a claimed excess of hot Jupiters around solar-mass stars, while the rate of giant planets at wider separations seems to be in agreement with field statistics (Brucalassi et al. 2014, 2016, 2017). At intermediate ages, RV surveys searching for hot Jupiters in the nearby Hyades (∼750 Myr) and Praesepe (∼790 Myr) clusters have resulted in varying degrees of success (Cochran et al. 2002; Quinn et al. 2012, 2014). More recently, RV monitoring has revealed a number of hot Jupiters orbiting T Tauri and post-T Tauri stars (Donati et al. 2016; Johns-Krull et al. 2016a; Yu et al. 2017).

As far as transit searches in clusters go, the majority of prior surveys were sensitive only to hot Jupiters yet still lacked the combination of sensitivity and sample size needed to distinguish differences in planet populations in clusters and the field (see Janes & Kim 2009, for a review of early cluster surveys). A meta-analysis of early transit searches within open clusters showed that the null results from those surveys were consistent with expectations from field statistics (van Saders & Gaudi 2011). To date, only a single survey has compared the cluster and field occurrence rates of planets smaller than Neptune. That work used *Kepler* observations of the ∼1 Gyr-old cluster NGC 6811 to find agreement between field and cluster rates, from two transiting planets around G-type stars (Meibom et al. 2013).

Compared with the *Kepler* mission, *K2* (Howell et al. 2014) has targeted a much more diverse set of astrophysical sources, enabling a wide range of Solar System, planetary, stellar, galactic, and extragalactic investigations. Since early 2014, *K2* has steadily assembled a legacy archive of precision photometry for more than 300,000 stars, including thousands of members of young clusters and associations. From these data, the first secure transiting planets in young (< 1 Gyr) clusters have been established. We summarize our current knowledge of young exoplanets detected via the transit or radial velocity methods in Table 1. For each of the clusters surveyed, the *K2* data are unprecedented in precision, cadence, baseline, and number of mem-

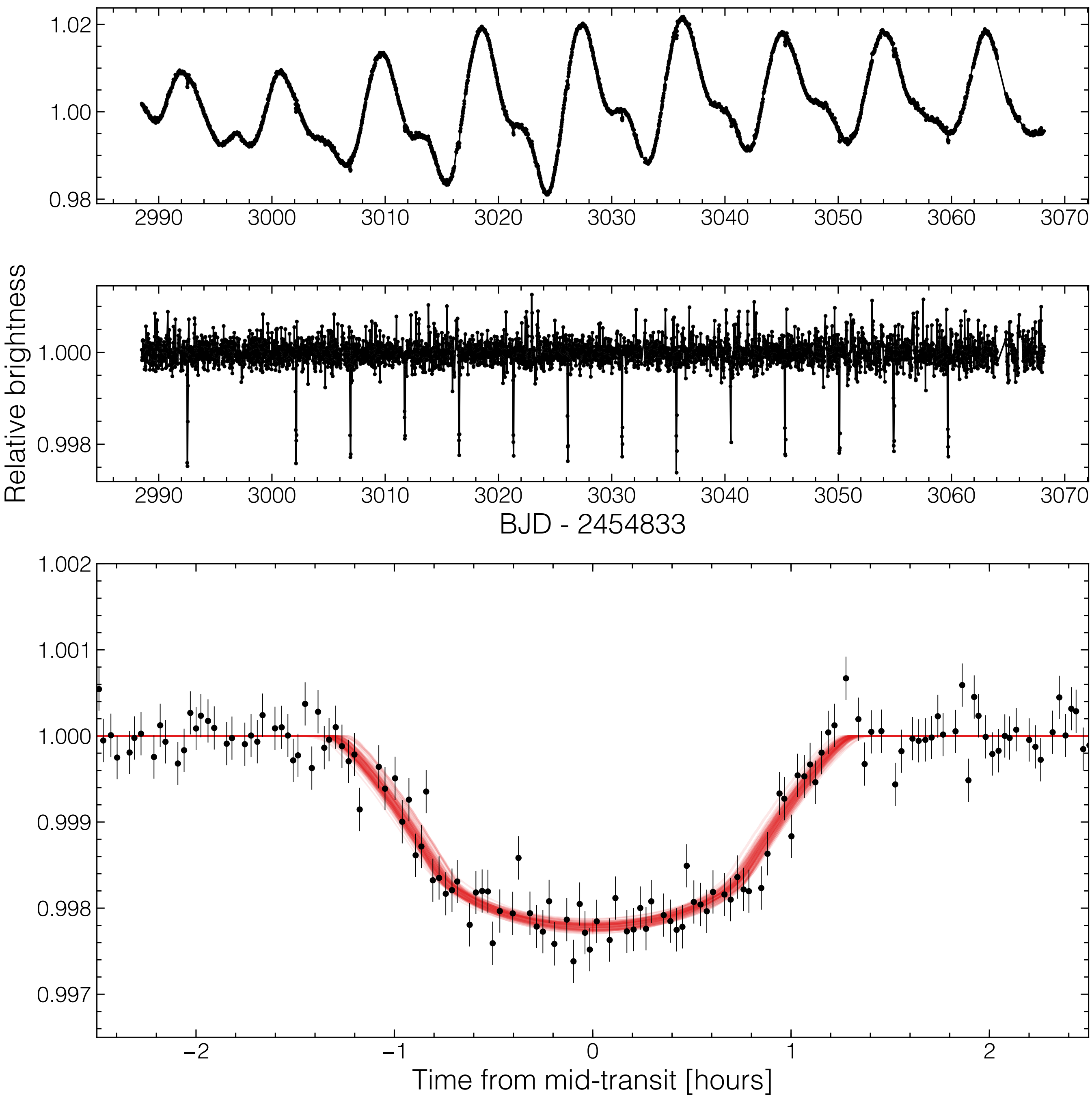

Figure 1. *K2* light curve of EPIC 247267267. In the top panel, the stellar variability pattern due to rotational modulation of starspots is apparent, as are the transits of EPIC 247267267 b. In the middle panel, the stellar variability has been removed. Missing transits are due to sections of the light curve that were removed in the detrending procedure. In the bottom panel, phase-folded model fits to the transits of EPIC 247267267 b. The red curves show 200 randomly selected models from the MCMC chain.

bers surveyed. Recently, Rizzuto et al. (2017) presented a uniform search for transits in the *K2* cluster data. Our group is also involved in a parallel effort to measure the completeness of those data, laying the foundation for comparative planet occurrence at young ages.

A handful of the young transiting planets found with *K2* seem anomalously large compared to close-in planets around field-age stars of a similar mass, a possible hint for ongoing radius evolution (Mann et al. 2017b). However, most of the cluster planets transit low-mass (mid-K and later type) stars where our knowledge of planet populations is more incomplete relative to the solar-type (FGK) stars targeted by *Kepler*. Thus, the question which must be answered is whether these planets are large because they are young, or whether we are only finding them because they are easier to detect. An important step in answering this question is to compare the densities between young and old planets, but to date none of the known young exoplanets have both radius and mass measurements.

Close-in sub-Neptunes with ages $\lesssim$100 Myr are particularly interesting, given theoretical predictions that their cores may continue to be cooling (Vazan et al. 2017) and the atmospheres of such planets should experience enhanced photo-evaporative mass-loss at early times (Owen & Wu 2013; Lopez & Fortney 2013; Chen & Rogers 2016). The bimodal radius distribution of close-in sub-Neptunes has been interpreted as evidence of photo-evaporative sculpting of this planet population (Fulton et al. 2017). Here we report the discovery and characterization of a sub-Neptune-sized planet transiting a likely member of the Cas-Tau association. It is one of the younger known transiting exoplanets and thus a useful benchmark for studying the evolution of close-in sub-Neptunes.

2. OBSERVATIONS

2.1. *K2 Photometry*

The *Kepler* space telescope observed EPIC 247267267 (K_P=12.811 mag) between UT 2017 March 8 and 2017 May 27 during Campaign 13 of the *K2* mission. Due to roll angle variations and non-uniform intra-pixel sensitivity, photometry from the *K2* mission contains systematic artifacts, which are often much larger in amplitude than planet transit signals or even the intrinsic stellar variability. We corrected for these systematic effects using the K2SC package (Aigrain et al. 2016), which simultaneously models time- and position-dependent flux variations using Gaussian process regression. From these data we discovered a periodic signal in a systematic search for transiting planets among the K2 C13 targets. We also extracted photometry from a small square aperture (Figure 2) and circular apertures of different radii to mitigate the impact of nearby stars. The transits of EPIC 247267267 b are recovered at a consistent depth within apertures between 4″ and 16″ in radius. This argues against the transit signal being due to a diluted eclipsing binary at a projected separation larger than 4″. We also constructed a separate light curve, initially correcting for systematics using the K2SFF routine (Vanderburg & Johnson 2014), and then using that preliminary correction as a starting point to produce a light curve by performing a simultaneous least-squares minimization (prior to the transit model-fitting stage) to the transits, stellar activity, and systematics after removing flares (following Vanderburg et al. 2016). We flattened the light curve by dividing away the best-fit stellar variability pattern from the light curve. This light curve proved to be of higher precision and we adopted it for the remaining analysis. From Box-fitting Least Squares periodogram analyses (Kovács et al. 2002) of light curves both including and excluding the transits of EPIC 247267267 b we find no evidence

Table 1. Known and proposed exoplanets in sub-Gyr populations detected via the transit or radial velocity method.

Parent Population	Age (Myr)	Planet	Host SpT	Period (d)	R_P ($R_\oplus$)	$M_P \sin i$ (M_{Jup})	Method	Year	Ref.
Taurus	≃2	V830 Tau b	M0	4.93	···	0.63 ± 0.11	RV	2016	1
Taurus	≃2	CI Tau b	K4IV	8.989	···	8.08 ± 1.53	RV	2016	2
Orion OB1a	≃2-3	CVSO 30 b	M3	0.448413	21.4 ± 2.4	<4.8 ± 1.2	transit	2012	3–10
Upper Sco	≃5–10	**K2-33 b**	M3	5.42513	5.8 ± 0.6	<3.6	transit	2016	11,12
Taurus	≃17	TAP 26 b	K7	10.79	···	1.66 ± 0.31	RV	2017	13
Cas-Tau	50–90	**EPIC 247267267 b**	K6.5	4.79507	$3.01^{+0.51}_{-0.48}$	<3	transit	2017	this work
AB Dor	149^{+51}_{-19}	BD+20 1790 b	K5Ve	7.78287	···	6.37 ± 1.35	RV	2010	14,15
Ursa Major	414 ± 23	HD 147513 b	G5V	528.4	···	1.21	RV	2004	16
Hyades	750 ± 100	ϵ Tau b	K0III	594.9	···	7.6 ± 0.2	RV	2007	17
Hyades	750 ± 100	HD 285507 b	K4.5V	6.0881	···	0.917 ± 0.033	RV	2014	18
Hyades	750 ± 100	**K2-25 b**	M4.5	3.484552	$3.43^{+0.95}_{-0.31}$	<3	transit	2016	19,20
Hyades	750 ± 100	**K2-136 b**	K5.5	7.975292	$0.99^{+0.06}_{-0.04}$	···	transit	2017	21–23
Hyades	750 ± 100	**K2-136 c**	K5.5	17.307137	$2.91^{+0.11}_{-0.10}$	···	transit	2017	21–23
Hyades	750 ± 100	**K2-136 d**	K5.5	25.575065	$1.45^{+0.11}_{-0.08}$	···	transit	2017	21–23
NGC 2423	790 ± 320	NGC 2423-3 b	A0	714	···	10.6	RV	2007	24
Praesepe	790 ± 60	Pr0201 b	F7.5	4.4264	···	0.540 ± 0.039	RV	2012	25
Praesepe	790 ± 60	Pr0211 b	G9.3	2.1451	···	1.844 ± 0.064	RV	2012	25
Praesepe	790 ± 60	Pr0211 c	G9.3	>3500	···	7.9 ± 0.2	RV	2016	26
Praesepe	790 ± 60	**K2-95 b**	M3	10.13509	3.7 ± 0.2	···	transit	2016	27–30
Praesepe	790 ± 60	**K2-100 b**	F8	1.673916	3.5 ± 0.2	···	transit	2016	28,29
Praesepe	790 ± 60	**K2-101 b**	K3	14.67729	2.0 ± 0.1	···	transit	2017	29
Praesepe	790 ± 60	**K2-102 b**	K4	9.9156	1.3 ± 0.1	···	transit	2017	29
Praesepe	790 ± 60	**K2-103 b**	K9	21.1696	2.2 ± 0.2	···	transit	2017	29
Praesepe	790 ± 60	**K2-104 b**	M1	1.97419	1.9 ± 0.2	···	transit	2016	28,29
Praesepe	790 ± 60	**EPIC 211901114**	M3	1.648932	9.6 ± 5.3	···	transit	2017	29

References. — 1. Donati et al. (2016); 2. Johns-Krull et al. (2016a); 3. van Eyken et al. (2012); 4. Barnes et al. (2013); 5. Yu et al. (2015); 6. Ciardi et al. (2015b); 7. Raetz et al. (2016); 8. Howarth (2016); 9. Johns-Krull et al. (2016b) 10. Onitsuka et al. (2017); 11. David et al. (2016a); 12. Mann et al. (2016a); 13. Yu et al. (2017); 14. Hernán-Obispo et al. (2010); 15. Hernán-Obispo et al. (2015); 16. Mayor et al. (2004); 17. Sato et al. (2007); 18. Quinn et al. (2014); 19. Mann et al. (2016b); 20. David et al. (2016a); 21. Ciardi et al. (2017); 22. Mann et al. (2017a); 23. Livingston et al. (2017); 24. Lovis & Mayor (2007); 25. Quinn et al. (2012); 26. Malavolta et al. (2016); 27. Obermeier et al. (2016); 28. Libralato et al. (2016); 29. Mann et al. (2017b); 30. Pepper et al. (2017)
Systems discovered from *K2* photometry are highlighted in bold.

for other periodic signals corresponding to additional transiting planets.

2.2. *Literature data*

To aid our stellar characterization process, we gathered astrometric and photometric data from the literature. These data included proper motions from the UCAC5 catalog (Zacharias et al. 2017) and broadband photometry from the *Gaia* DR1 (Gaia Collaboration et al. 2016a,b), *GALEX* DR5 (Martin et al. 2005), APASS DR9 (Henden et al. 2016), 2MASS (Cutri et al. 2003), and AllWISE (Cutri & et al. 2013) catalogs. The photometric and astrometric properties of EPIC 247267267 are summarized in Table 2.

2.3. *Adaptive optics imaging*

Adaptive optics imaging of EPIC 247267267 at K_s filter ($\lambda_\circ = 2.159; \Delta\lambda = 0.011$ μm) was acquired with the ShARCS infrared camera behind the ShaneAO adaptive optics system on the Lick 3-m telescope on 31 August 2017 UT. The ShARCS camera has an unvignetted field of view approximately 20″ and has a pixel scale of 0.033″ pixel^{-1}. The AO data were obtained in a 9-point dither pattern with dither point separated by 5″ and a 60 s integration time per frame for a total of 540 s. We used the dithered images to remove sky background and dark current, and then align, flat-field, and stack the individual images. The resolution of the Lick

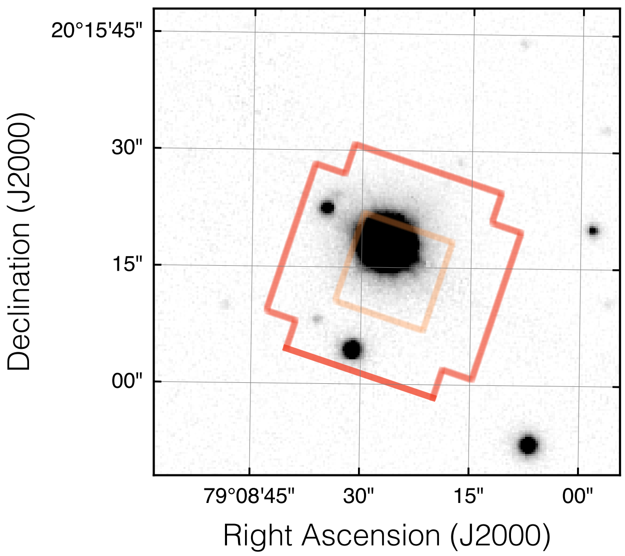

Figure 2. Pan-STARRS r-band image centered on EPIC 247267267 showing the adopted *K2* aperture in red and a smaller aperture in orange, from which the transits were also recovered at a consistent depth. We also inspected photometry from 4″ wide square apertures centered on the neighboring stars to the south and to the east to confirm that neither are eclipsing binaries.

Table 2. Astrometry and Photometry of EPIC 247267267

Parameter	Value	Source
Astrometry		
α R.A. (hh:mm:ss)	05:16:33.76	EPIC
δ Dec. (dd:mm:ss)	20:15:18.39	EPIC
μ_α (mas yr^{-1})	24.3 ± 1.2	UCAC5
μ_δ (mas yr^{-1})	-45.4 ± 1.2	UCAC5
Photometry		
NUV (mag)	21.688 ± 0.364	*GALEX* DR5
B (mag)	14.713 ± 0.006	APASS DR9
V (mag)	13.322 ± 0.015	APASS DR9
G (mag)	12.715 ± 0.002	*Gaia* DR1
g' (mag)	14.089 ± 0.034	APASS DR9
r' (mag)	12.758 ± 0.038	APASS DR9
i' (mag)	12.230 ± 0.011	APASS DR9
J (mag)	10.868 ± 0.024	2MASS
H (mag)	10.206 ± 0.025	2MASS
K_s (mag)	10.058 ± 0.018	2MASS
$W1$ (mag)	9.975 ± 0.023	AllWISE
$W2$ (mag)	10.007 ± 0.020	AllWISE
$W3$ (mag)	9.902 ± 0.060	AllWISE
$W4$ (mag)	>8.961	AllWISE

imaging was 0.25″ (FWHM) with a detection contrast of 2.8 magnitudes at one FWHM separation from the target.

To obtain a higher resolution and deeper image, we also observed EPIC 247267267 with infrared high-resolution adaptive optics (AO) imaging, both at Keck Observatory and Lick Observatory. The Keck Observatory observations were made with the NIRC2 instrument on Keck-II behind the natural guide star AO system. The observations were made on 2017 Oct 31 in the narrow-band $Br-\gamma$ filter ($\lambda_o = 2.1686\mu$m, $\Delta\lambda = 0.0326\mu$m) in the standard 3-point dither pattern that is used with NIRC2 to avoid the left lower quadrant of the detector which is typically noisier than the other three quadrants. The dither pattern step size was 3″ and was repeated three times, with each dither offset from the previous dither by 0.5″. The observations utilized an integration time of 10 seconds with one coadd per frame for a total of 90 seconds. The camera was in the narrow-angle mode with a full field of view of 10″ and a pixel scale of approximately 0.1″ per pixel. The resolution of the Keck imaging was 0.06″ (FWHM) with a detection contrast of 3.5 magnitudes at one FWHM separation from the target.

The sensitivity of the final combined AO images were determined by injecting simulated sources separated from the primary target in integer multiples of the central source FWHM. The brightness of each injected source was scaled until standard aperture photometry detected the injected source with 5σ significance. The resulting brightness of the injected sources relative to the primary target set the 5σ con-

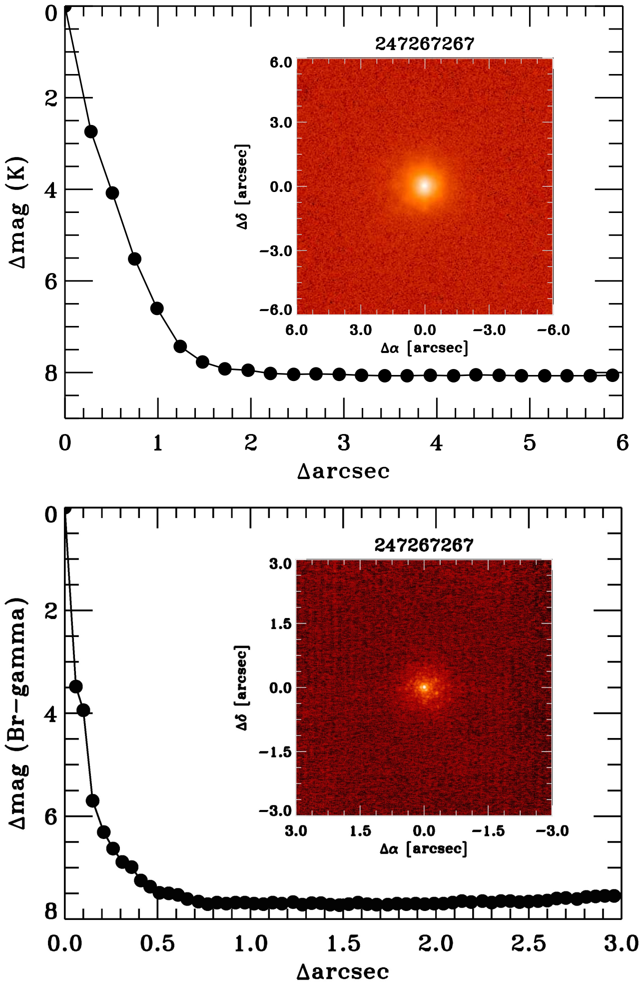

Figure 3. Contrast sensitivity and inset image of EPIC 247267267 in K_s as observed with the Lick Observatory 3m Shane adaptive optics system (above) and in Br-γ from the NIRC2 camera on the Keck-II telescope (below). In each case the 5σ contrast limit in Δ-magnitude is plotted against angular separation in arcseconds.

trast limits (see Figure 3). We find no evidence for nearby stars brighter than $\Delta K_s \approx 4$ mag outside of $0.5''$, which corresponds to a K_p limit of ≈ 6 mag, using the $K_p - K_s$ empirical relation for dwarf stars (Howell et al. 2012), and is used to set the limits on the dilution of the observed transit (Ciardi et al. 2015a) for the false-positive assessment (see below).

2.4. *Keck-I/HIRES*

High-dispersion spectra of EPIC 247267267 were acquired on UT 2017 Aug 29 and Nov 8 using the HIRES spectrograph (Vogt et al. 1994) on the Keck-I telescope. The spectra were obtained with the C2 decker, providing a spectral resolution of $R \approx 50000$ in the range of ∼3640–7990Å. The achieved SNR was 32/pixel at the peak of the blaze function near 5500Å. The star's radial velocity (RV) was measured from the HIRES spectra using the telluric A and B absorption bands as a wavelength reference (Chubak et al. 2012). These RVs are accurate at the ∼200 m s^{-1} level, which we adopt as the uncertainty on each telluric RV measurement. From the HIRES spectra we also derived stellar parameters which we adopted for the remaining analysis. Our stellar characterization procedures are described in § 3.4 and summarized in Table 5. The RV measurements from HIRES and TRES (described below) are reported in Table 3.

2.5. *TRES*

Using the Tillinghast Reflector Echelle Spectrograph (TRES) on the 1.5m telescope at Fred L. Whipple Observatory, we observed EPIC 247267267 on UT 2017 Sep 29. The resolution of this spectrum is $R \approx 44000$ between 3850–9096 Å. From a 2600s integration, the achieved SNR is 18.9 per pixel at 5110 Å. We measured spectroscopic parameters and the absolute RV for EPIC 247267267 from the TRES spectrum using the Stellar Parameter Classification (SPC) tool (Buchhave et al. 2012, 2014). SPC measures RV from cross-correlating Kurucz (1992) synthetic template spectra with the target spectrum, allowing for rotational line broadening. We adopt an error of 0.2 km s^{-1} in the TRES RV, which is mainly due to the uncertainty in transforming the RV onto the IAU absolute velocity scale. The spectroscopic parameters found with SPC are broadly consistent

Table 3. Radial velocities of EPIC 247267267

UT Date	BJD	RV (km s^{-1})	Instrument
2017 Aug 29	2457995.120599	16.85 ± 0.20	HIRES
2017 Sep 29	2458025.897972	17.23 ± 0.20	TRES
2017 Nov 08	2458066.060714	16.80 ± 0.20	HIRES

with those found from the HIRES spectrum (see § 3.4).

3. ANALYSIS

3.1. *Transit model fitting*

We used the BATMAN package (Kreidberg 2015), based on the Mandel & Agol (2002) formalism, to generate transit models and fit these to the *K2* photometry. Parameter uncertainties were estimated through Markov chain Monte Carlo (MCMC) analysis using the EMCEE package (Foreman-Mackey et al. 2013). The free parameters in the transit fits are the orbital period ($P_{\rm orb}$), the time of mid-transit (T_0), the fractional stellar radius (R_*/a), the planet-star radius ratio (R_p/R_*), eccentricity (e) and the longitude of periastron (ω). We first performed a fit assuming a circular orbit, then relaxed this assumption and allowed eccentricity and the longitude of periastron to be free parameters. Transit models were numerically integrated to match the *Kepler* long cadence (1766 s) prior to fitting. The median parameters of the transit fits determined from the MCMC chain and the uncertainties, determined from the 16% and 84% quantiles, are reported in Table 4. For both fits we used 80 walkers with 4500 steps each and discarded the first 500 burn-in steps to mitigate the impact of our initial parameter estimates. For the eccentric fit, we assumed a Gaussian prior on the mean stellar density centered at 3.49 g cm^{-3} with width 2.64 g cm^{-3}. In both fits we assumed quadratic limb darkening parameters with uniform priors centered

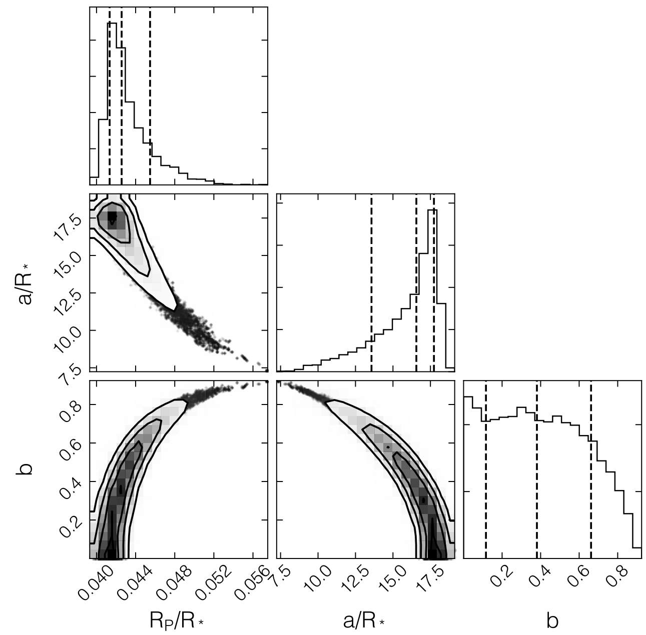

Figure 4. Joint parameter distributions from the MCMC transit fit in the circular case.

on $a_{\rm LD}$=0.7129 and $b_{\rm LD}$=0.0229 with widths of 0.11 and 0.036 respectively. The choice of limb-darkening values was based on our atmospheric parameters and interpolating between the tables of Claret et al. (2012). We found our model fitting, and hence overall conclusions, to be relatively insensitive to the precise choice of limb-darkening parameters. From the directly fitted parameters in the MCMC analysis, we derived the transit duration and mean stellar density using equations (3) and (19) from Seager & Mallén-Ornelas (2003), respectively. The mean stellar density clearly indicates the planet is orbiting a dwarf star and not a giant, but we can not rule out that the star is at the end of the pre-main-sequence phase of contraction. We note the equation for mean stellar density assumes a circular orbit, but the general conclusion remains unchanged given the vast difference in stellar densities for dwarfs and giant stars. Transit model fits to the *K2* light curve are shown in Figure 1 and joint parameter distributions from the MCMC chain are shown in Figure 4.

Table 4. Results of EPIC 247267267 b transit fits

Parameter	Value (Fit 1)	Value (Fit 2)
Directly determined parameters		
Orbital period, $P_{\rm orb}$ (days)	$4.79507^{+0.00013}_{-0.00013}$	$4.79507^{+0.00014}_{-0.00013}$
Time of mid-transit, T_0 (BJD-2400000)	$57859.11304^{+0.00056}_{-0.00055}$	$57859.11317^{+0.00072}_{-0.00067}$
Radius ratio, R_P/R_*	$0.0426^{+0.0029}_{-0.0012}$	$0.0423^{+0.0017}_{-0.0010}$
Scaled semi-major axis, a/R_*	$16.6^{+1.2}_{-3.0}$	$14.8^{+2.2}_{-3.3}$
Impact parameter, b	$0.38^{+0.28}_{-0.27}$	$0.32^{+0.24}_{-0.22}$
Total duration, T_{14} (hours)	$2.154^{+0.061}_{-0.046}$	$2.37^{+0.59}_{-0.22}$
Inclination, i (degrees)	$88.69^{+0.94}_{-1.49}$	$88.5^{+1.1}_{-1.9}$
Eccentricity, e	0.0 (fixed)	$0.18^{+0.25}_{-0.13}$
Longitude of periastron, ω (degrees)	0.0 (fixed)	77^{+98}_{-59}
Mean stellar density, ρ_* (g cc^{-1})	$3.74^{+0.85}_{-1.69}$	...
Limb darkening coefficient, $a_{\rm LD}$	$0.688^{+0.077}_{-0.058}$	$0.683^{+0.081}_{-0.057}$
Limb darkening coefficient, $b_{\rm LD}$	$0.020^{+0.026}_{-0.023}$	$0.024^{+0.023}_{-0.025}$
Derived parameters		
Planet radius, R_P ($R_\oplus$)^a	$3.01^{+0.51}_{-0.48}$	$2.97^{+0.48}_{-0.47}$
Semi-major axis, a (AU)	$0.0482^{+0.0012}_{-0.0013}$	$0.0482^{+0.0012}_{-0.0013}$
Insolation flux, S ($S_\oplus$)	$45.3^{+14.9}_{-14.7}$	$45.2^{+15.0}_{-14.8}$
Equilibrium temperature, $T_{\rm eq}$ (K)^b	655^{+68}_{-26}	692^{+93}_{-48}

(a) The planet radius does not account for dilution from nearby stars within the photometric aperture, and may be negligibly larger by ≈1.2%.
(b) The equilibrium temperature is calculated assuming an albedo of 0.3.

3.2. *False positive assessment*

Two nearby stars within 15″ of EPIC 247267267 are contained within our photometric aperture. The Pan-STARRS survey (Chambers et al. 2016; Flewelling et al. 2016) measured these sources, PSO J051634.085+201504.266 and PSO J051634.329+201522.312, to be approximately 4.42 mag and 5.52 mag fainter than EPIC 247267267 at r band, respectively. From equation (7) of Ciardi et al. (2015a) we calculated that the flux dilution from these nearby stars affects the inferred planet radius at a level of ≈1.2%, such that the true planet radius is negligibly larger than quoted. Here we are not concerned with this dilution, but with the possibility that this source or any other background source might be a contaminating eclipsing binary (EB) that is being diluted by EPIC 247267267. The transit signature can be recovered with a consistent depth from photometry extracted using a 4″ radius aperture, though at lower signal-to-noise due to the difficulties of detrending in the face of increased aperture losses. This effectively argues against the possibility of the nearby star being a background EB, since its light should not contami-

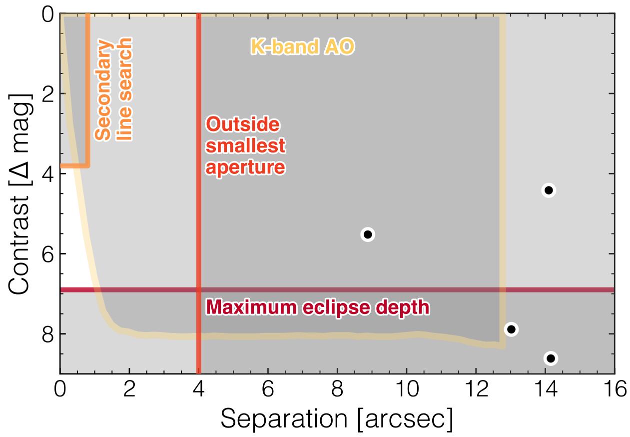

Figure 5. Contrast versus projected angular separation. The grey shaded regions show the excluded areas of parameter space in which a putative false positive could reside. The black points show nearby sources detected by Pan-STARRS. Note the secondary line search is blind to companions with velocity separations <15 km s^{-1} from the primary.

nate the photometry extracted from the smaller aperture. Other nearby stars within 16″ either reside outside our aperture or are too faint to explain the observed transit depth (Figure 5).

In principle, an EB can dim by a maximum of 100% (although such systems are rare). The observed transit depth thus sets a limit on the faintness of a diluted EB of approximately $\Delta K_p \lesssim 6.9$ mag. In the simplified case of a target star with constant flux and a contaminating EB contained in the same photometric aperture, the observed depth of a diluted eclipse neglecting sky background is $\delta_{\rm obs} = \delta_{\rm ecl}\Delta F/(1+\Delta F)$, where ΔF is the flux ratio between the target and the contaminating EB in the observed bandpass, and $\delta_{\rm ecl}$ is the intrinsic eclipse depth of the EB. In this case, if the nearby star is in fact an EB, only eclipses with depths greater than $\approx 28\%$ depth are capable of producing the observed transit depth. We extracted photometry from small apertures centered on the neighboring stars to the south and to the east, finding no evidence for dimmings of a depth greater than the observed transit depth and at the period of EPIC 247267267 b. We have thus ruled out the possibility that either of the neighboring stars are EBs with periods comparable to the period of EPIC 247267267 b.

Using the TRILEGAL galactic model (Girardi et al. 2005), we simulated a 1-deg^2 field in the direction of EPIC 247267267. From the simulated field, we calculated the expected colors and surface density of background stars bright enough to produce the observed transit depth (i.e. $V \lesssim 20.2$ mag). We then scaled the resulting surface density by the size of the *K2* aperture to estimate the total number of expected contaminants. We found that < 0.4 putative contaminants are expected within a 12″ aperture or < 0.2 within an 8″ aperture. The number of expected contaminants that would be EBs is even smaller. The mean near-IR colors of putative contaminants in the simulated field are $(J-H)$=0.49 mag and $(H-K)$=0.08 mag, suggestive of a K-type dwarf or giant. As noted earlier, the mean stellar density from the transit fit effectively rules out the possibility of a planet transiting a giant star.

We searched for secondary spectral lines in the HIRES spectrum from 2017 Aug 29 using the procedure described in Kolbl et al. (2015). We found no evidence for a nearby star down to 3% the brightness of the primary and within 0.8″. Notably, this method is blind to companions with velocity separations <15 km s^{-1}. We show the excluded regions of parameter space for hypothetical false positive scenarios in Figure 5.

We also quantified the false positive probability (FPP) using the `vespa` software package (Morton 2015). From the input *K2* photometry, the star's spectroscopic parameters and photometry, and high resolution imaging constraints (the ShaneAO K-band contrast curve, in this case), `vespa` evaluated the relative likelihoods of transiting planet scenarios versus various diluted eclipsing binary scenarios. The soft-

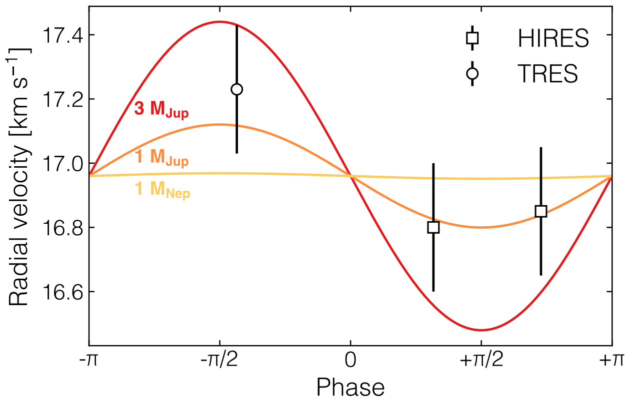

Figure 6. Radial velocities phased to the orbital ephemeris of EPIC 247267267 b. We find no evidence for orbital motion and from these measurements place an upper limit to the planet's mass of $<3\ M_{\rm Jup}$ at 95% confidence. The expected RV curves for planet masses corresponding to Neptune, Jupiter, and three times the mass of Jupiter are shown by the colored curves.

ware accounts for binary population statistics and the ambient surface density of stars using the TRILEGAL galactic model. We found an overall false positive probability of 1/153, with the primary contributor to the FPP being an EB at twice the inferred period. In this case, one might expect differences in the depths of "odd" and "even" transits, so long as the hypothetical background EB has different primary and secondary eclipse depths.

As with any transiting planet candidate lacking a mass measurement, it is difficult to rule out all hypothetical false positive scenarios. Nevertheless, from the qualitative arguments presented above and the quantitative VESPA light curve analysis, we conclude that a transiting planet around EPIC 247267267 is the most secure interpretation for the *K2* signal.

3.3. *Upper limit to the planet mass*

From three RV measurements we find no evidence for orbital motion corresponding to Doppler semi-amplitudes greater than ∼200 m s^{-1} at the period of the planet (Figure 6). All three measurements are also consistent with being equal at the ≈1σ level. From these three measurements we performed a one parameter MCMC fit to determine an upper limit to the Doppler semi-amplitude and thus the planet's mass. We performed these fits using the `radvel` package(Fulton et al. 2018)[1], fixing the planet's ephemeris to that determined from the transit fits and assuming a circular orbit. We did not allow for RV jitter nor did we allow for any systematic offset between the HIRES and TRES RVs, as no such offset should exist. We fixed the systemic velocity to the value reported in Table 5. From this fit we determined an upper limit to the mass of EPIC 247267267 b of $<3\ M_{\rm Jup}$ at 95% confidence, which rules out the possibility that a stellar or brown dwarf companion is responsible for the transits.

3.4. *Stellar characterization*

Below we discuss the various procedures used to characterize the host star. Unless otherwise noted, our quoted uncertainties in the non-spectroscopic parameters were derived through Monte Carlo simulations assuming normally distributed errors in the input parameters. Our spectroscopic analysis points to a dwarf-like gravity suggesting that the star is on or very nearly on the ZAMS. The theoretical pre-main-sequence lifetime of a 0.65 $M_\odot$ star (corresponding to our adopted mass) is ∼110 Myr (see Figure 7). If EPIC 247267267 is in fact at the very end of its pre-main-sequence contraction the true radius would still be encompassed by our radius uncertainties. Thus, our stellar characterization procedures are valid in employing spectral templates of field-aged stars as well as empirical relations based on field star properties. The stellar parameters resulting from our characterization are reported in Table 5.

Radius, effective temperature, and metallicity. From the HIRES spectrum, we

[1] https://github.com/California-Planet-Search/radvel

Table 5. Parameters of EPIC 247267267

Parameter	Value	Source
Kinematics and position		
Barycentric RV (km s^{-1})	16.96 ± 0.19	HIRES, TRES
U (km s^{-1})	-15.1 ± 1.3	
V (km s^{-1})	-20.1 ± 1.7	
W (km s^{-1})	-5.0 ± 1.3	
Kinematic distance (pc)	79^{+11}_{-9}	
Measured parameters		
$T_{\rm eff}$ (K)	**4108 ± 70**	HIRES+SpecMatch-Emp
	4288 ± 50	TRES+SPC
R_* ($R_\odot$)	**0.64 ± 0.10**	HIRES+SpecMatch-Emp
$\log g$ (dex)	4.739 ± 0.10	TRES+SPC
[Fe/H] (dex)	**-0.06 ± 0.09**	HIRES+SpecMatch-Emp
[M/H] (dex)	-0.382 ± 0.08	TRES+SPC
$v \sin i_*$ (km s^{-1})	**3.54 ± 0.50**	TRES+SPC
	3–4	HIRES+SpecMatch-Emp
$\log R'_{HK}$ (dex)	-3.9 ± 0.5	HIRES
S-index	5 ± 1	HIRES
Rotation period (days)	8.88 ± 0.40	*K2*
Derived parameters		
A_V (mag)	0.27 ± 0.05	$T_{\rm eff}$, $B-V$, PM13
R_* ($R_\odot$)	0.633 ± 0.031	$T_{\rm eff}$, B12
M_* ($M_\odot$)	**0.65 ± 0.05**	$T_{\rm eff}$, L_*
	0.53 ± 0.05	$M_{\rm K_s}$, M15
L_* ($L_\odot$)	**0.105 ± 0.034**	$T_{\rm eff}$, R_*
	0.107 ± 0.013	$T_{\rm eff}$, B12
Estimated age		
$\tau_{\rm isoc,1}$ (Myr)	171^{+684}_{-131}	$T_{\rm eff}$, L_*
$\tau_{\rm isoc,2}$ (Myr)	156^{+2414}_{-126}	$T_{\rm eff}$, ρ_*
$\tau_{\rm gyro,1}$ (Myr)	124^{+13}_{-15}	$P_{\rm rot}$, $(B-V)_0$, B07
$\tau_{\rm gyro,2}$ (Myr)	262^{+35}_{-41}	$P_{\rm rot}$, $(B-V)_0$, MH08
$\tau_{\rm R'_{HK}}$ (Myr)	139^{+1353}_{-119}	$\log R'_{HK}$, MH08
$\tau_{\rm NUV}$ (Myr)	111^{+160}_{-65}	$(NUV-J)_0$, $(J-K)_0$, F11
τ_* (Myr)	150^{+350}_{-100}	
$\tau_{\rm Cas-Tau}$ (Myr)	46 ± 8	

Where multiple values for a parameter are reported, our adopted value is in boldface. PM13: Pecaut & Mamajek (2013); B12: Boyajian et al. (2012); M15: Mann et al. (2015); B07: Barnes (2007); MH08: Mamajek & Hillenbrand (2008); F11: Findeisen et al. (2011).

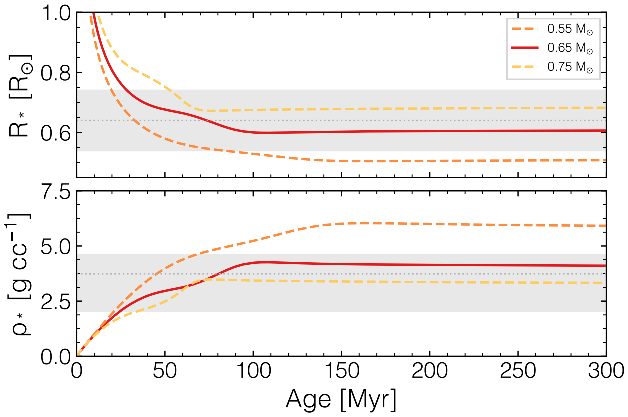

Figure 7. Theoretical predictions from the MIST models (Choi et al. 2016) of the evolution in radius (upper panel) and mean stellar density (lower panel) for low-mass stars. The grey lines and shaded regions show the adopted stellar radius and the mean stellar density measured from the transit fit.

determined the stellar $T_{\rm eff}$ (4108 ± 70 K), radius (0.64 ± 0.10 $R_\odot$), and [Fe/H] (-0.06 ± 0.09 dex) using the SpecMatch-Emp pipeline (Yee et al. 2017). SpecMatch-Emp uses a library of HIRES spectra for benchmark stars with securely measured parameters (via interferometry, asteroseismology, LTE spectral synthesis, and spectrophotometry) to find the optimal linear combination of these templates that matches a target spectrum. The parameters of the target star are determined via interpolation between the parameters for the templates in the optimal linear combination. The spectroscopic temperature from the TRES spectrum and the SPC analysis is marginally discrepant with that found from SpecMatch-Emp ($T_{\rm eff,SPC}$ = 4288 ± 50 K) and the metallicity is also much lower ([M/H]$_{\rm SPC}$ = -0.382 ± 0.08 dex). We do not have a satisfactory explanation for these differences, but they may be attributed to the different approaches of the methods. SPC uses synthetic Kurucz (1992) spectral templates, while SpecMatch-Emp uses empirical spectral templates from benchmark stars. The metallicity measured with SpecMatch-Emp should be regarded with caution as the empirical templates in this temperature range do not sample an evenly-spaced range of metallicities. Notably, the $(V-K_s)$ color of the star (3.264 ± 0.023 mag) suggests $T_{\rm eff}$ = 4150 ± 16 K when interpolating between the values in Table 5 of Pecaut & Mamajek (2013), and the $(V-J), (r-J), (r-z)$ colors and [Fe/H] imply $T_{\rm eff}$ = 4180 ± 40 K when using the empirical relations of Mann et al. (2015). These photometric $T_{\rm eff}$ estimates do not account for reddening.

Spectral type and extinction. The best-matching template star from the SpecMatch-Emp analysis is GJ 3494, which has been assigned spectral types of M0 and K5 (Skiff 2014). From the spectroscopically determined $T_{\rm eff}$ and the empirical spectral-type-$T_{\rm eff}$ relations presented in Pecaut & Mamajek (2013), hereafter PM13, we find the $T_{\rm eff}$ to be consistent with a spectral type of K6.5. Given the stellar effective temperature, we interpolated between the intrinsic color tables of PM13 to determine an expected intrinsic color of $(B-V)_0 =$ 1.305 mag, corresponding to a color excess of $E(B-V) = 0.086 \pm 0.016$ mag. We then assumed the Cardelli et al. (1989) extinction curve to derive A_V. We used the $(B-V)$ color excess above and the extinction coefficients derived by Yuan et al. (2013) for the *GALEX* and 2MASS passbands to derive near-UV and near-IR colors, which we later use to estimate the stellar age, as described in § 3.6.

Mass and luminosity. We derived the luminosity using the spectroscopically determined $T_{\rm eff}$, radius and the Stefan-Boltzmann Law. We derived a separate luminosity estimate from an empirical $T_{\rm eff}$-luminosity relation based on interferometry of low-mass stars (Boyajian et al. 2012). This second estimate is not entirely independent of the first estimate, since the spectroscopic parameter pipeline is calibrated to the same interferometric standards, among other benchmark stars. We derived a model-dependent mass from a theoretical H-R diagram using the solar-metallicity (Z=0.0152) PARSECv1.2S models (Bressan et al. 2012; Chen et al. 2014), our spectroscopically determined $T_{\rm eff}$, and the Stefan-Boltzmann determined luminosity. We also derived a distance-dependent mass from the kinematic distance, the apparent K_s magnitude, and a semi-empirical mass-$M_{\rm K_s}$ relation (Mann et al. 2015). Notably, this mass is 2σ lower than the model-dependent mass we adopt. We assume the discrepancy is due to the uncertainty in the distance. If the mass estimate from this empirical relation is correct, the mean stellar density from the transit fit would seem to reinforce the notion that the star is still on the pre-main-sequence. However, as a sanity check we compared our stellar parameters with those of the nearly equal-mass benchmark eclipsing binary GU Boo (López-Morales & Ribas 2005), which agree reasonably well with our adopted mass, radius, and temperature.

Rotation period and projected rotational velocity. A period of 8.88 $\pm$ 0.40 d, which we attribute to surface rotation of the star, was measured from a Lomb-Scargle periodogram analysis (Lomb 1976; Scargle 1982) of the *K2* light curve (Figure 8). The uncertainty in the rotation period was estimated from the standard deviation of a Gaussian fit to the oversampled periodogram peak. This uncertainty is likely overestimated, but encompasses the more difficult to quantify uncertainty in the rotation period due to e.g. differential rotation. The formal uncertainty, estimated by the periodogram peak width divided by the peak signal-to-noise, is 0.0085 d. A second peak in the periodogram at 4.41 $\pm$ 0.11 d is a harmonic of the true rotation period. The projected rotational velocity, $v_* \sin i_*$ = 3.54 $\pm$ 0.50 km s^{-1}, was measured from the TRES spectrum by broadening synthetic template spectra to match the observations. An independent and consistent

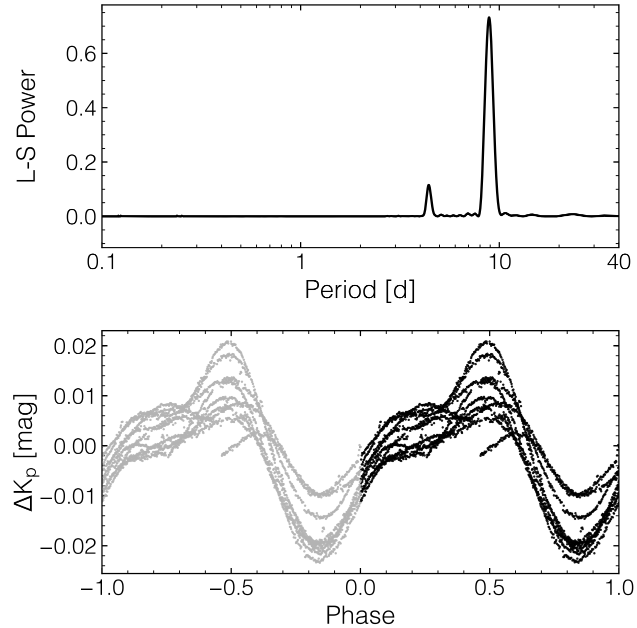

Figure 8. Lomb-Scargle periodogram from *K2* photometry of EPIC 247267267 (top) and the light curve phased to the rotation period of 8.88 d (bottom).

$v_* \sin i_*$ estimate of 3–4 km s^{-1} was found from the HIRES spectrum and SpecMatch-Emp by broadening empirical template spectra, assuming the template stars were not rotating. Using the TRES value and the *K2* rotation period we estimated the minimum stellar radius, $R_* \sin i_*$ = 0.621 $\pm$ 0.092 $R_\odot$. This value is within the uncertainty of our adopted radius, suggesting the stellar spin-axis is nearly edge-on. Put another way, for our adopted radius, the measured photometric rotation period, and assuming a uniform distribution in $\cos i_*$, the median and 68% confidence interval predicted for $v_* \sin i_*$ is 3.6 $\pm$ 0.6 km s^{-1}, in good agreement with our measurements.

Kinematics, Membership & Distance. The EPIC catalog contains a preliminary photometric distance estimate of 84^{+18}_{-11} pc, assuming the star is on the main sequence (Huber et al. 2016). *Are there any nearby young stellar populations that EPIC 247267267 might be a kinematic member of which could help in con-*

straining its age? EPIC 247267267 occupies a busy region of sky with regard to nearby young stellar populations. Within 200 pc and within 30° of EPIC 247267267's position are three open clusters (Hyades, 32 Ori & Pleiades), the Tau-Aur association, the Cas-Tau association, and the recently identified 118 Tau group. The best available proper motion for EPIC 247267267 is from the new UCAC5 catalog which factors in the new Gaia DR1 epoch: μ_α, μ_δ = 24.3, -45.4 (±1.2, ±1.2) mas yr^{-1} (Zacharias et al. 2017). Other recent estimates from the HSOY, URAT1, UCAC4, PPMX, and PPMXL catalogs are in good agreement given their larger uncertainties (∼2-6 mas yr^{-1}). The UCAC5 proper motion was compared to the proper motions and radial velocities of members of these groups from the literature. EPIC 247267267's proper motion is clearly inconsistent with the nearby 118 Tau group (μ_α, μ_δ = 4, -39 mas yr^{-1}). Although EPIC 247267267's radial velocity (16.96 ± 0.19 km s^{-1}) is similar to that of the Tau-Aur association (+16 km s^{-1}, Luhman et al. 2009), its proper motion is very different compared to the mean proper motion for the group (μ_α, μ_δ = 6, -21 mas yr^{-1}, or any of the subgroups (Luhman et al. 2009).

The only group which provides a near match of proper motion and radial velocity is the Cas-Tau association. Using the methodology of Mamajek (2005), the UCAC5 proper motion for EPIC 247267267 and the "spaghetti" velocity solution from de Zeeuw et al. (1999), we find the bulk of EPIC 247267267's proper motion is moving towards the Cas-Tau convergent point ($\mu_\upsilon = 51.3 \pm 1.2$ mas yr^{-1}) with negligible perpendicular motion ($\mu_\tau = 4.7 \pm 1.2$ mas yr^{-1}). The predicted kinematic distance is 79 ± 10 pc (kinematic parallax $\varpi = 12.7 \pm 1.6$ mas), with predicted radial velocity $v_r = 15.4$ km s^{-1} (compared to our measured value of 16.96 ± 0.19 km s^{-1}), and predicted peculiar motion 1.7 ± 0.5 km s^{-1}. Notably, de Zeeuw et al. (1999) adopted 3 km s^{-1} as the 1D velocity dispersion.

de Zeeuw et al. (1999) estimated the space velocity of Cas-Tau using the spaghetti method with their *Hipparcos* membership to be U, V, W = -13.24, -19.69, -6.38 km s^{-1} (U positive towards Galactic Center). As a check, and to provide a modern estimate, we cross-referenced de Zeeuw's membership of Cas-Tau members with the revised *Hipparcos* catalog (van Leeuwen 2007), *Gaia* DR1 (preferred, when available), and the radial velocity compilation of Gontcharov (2006). This provided UVW velocity estimates for 48 candidate Cas-Tau members. These are plotted in Fig. 9 along with the mean velocities for the Cas-Tau group from de Zeeuw et al. (1999) and the α Persei cluster, along with the estimate for EPIC 247267267 assuming the kinematic distance estimate of 79^{+11}_{-9} pc. The median UVW for the 48 members is U, V, W = -14.7±0.9, -21.3±0.8, -7.1±0.4 km s^{-1}. Using the probit method, which is resilient to the effects of extreme values, the 1σ scatters reflecting the core of the velocity distributions are estimated as 3.9, 3.7, 2.7 km s^{-1}). Accounting for the mean UVW velocity component uncertainties (2.4, 1.9, 1.4 km s^{-1}), this suggests the intrinsic U, V, W velocity dispersions among the de Zeeuw et al. Cas-Tau membership to be approximately 3.0, 3.1, and 2.2 km s^{-1}. This is likely reflecting the adopted 3 km s^{-1} velocity dispersion used by de Zeeuw et al. in their original kinematic membership selection. Further work is needed to clarify the membership of Cas-Tau with *Gaia* astrometry, and to search for kinematic and age substructure, however this is beyond the scope of this study.

3.5. *The Cas-Tau Association*

Cas-Tau was first formally proposed as an association by Blaauw (1956), based on the common motions of 49 B-stars covering a remarkably large patch of sky of about 100° × 140°.

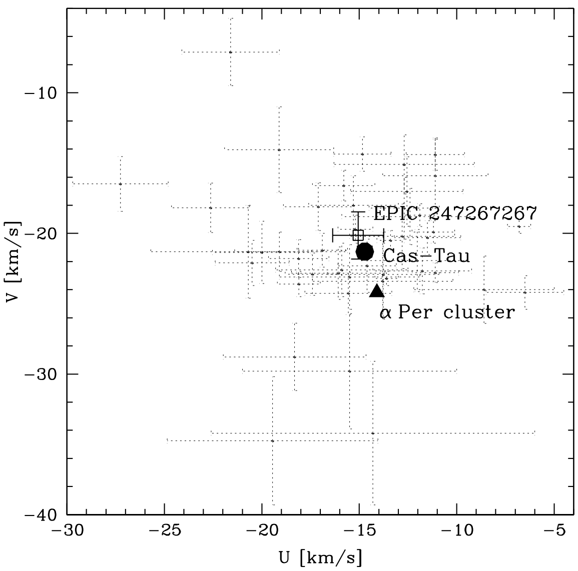

Figure 9. UV space motions for Cas-Tau (filled circle; from de Zeeuw et al. (1999) using the spaghetti method), α Per cluster (filled triangle; based on proper motion and RV from Robichon et al. (1998), mean position from Madsen et al. (2002), and distance from de Zeeuw et al. (1999)), and EPIC 247267267 (open square) assuming a kinematic distance of 79^{+11}_{-9} pc. The dashed crosses are revised velocity estimates (reflecting 1σ uncertainties) for de Zeeuw et al. (1999) Cas-Tau members using best available parallax from either revised Hipparcos data (van Leeuwen 2007) or *Gaia* DR1, combined with RVs from compilation of Gontcharov (2006).

The association shares motions with and spatially surrounds the α Persei (Per OB3) cluster, which led Blaauw to suggest a common origin for the two groups. Indeed, Rasmuson (1921) had already noted the kinematic group was not limited to the central α Per cluster, but that several other B- and A-stars formed a co-moving stream extending well beyond the cluster core. In the years following Blaauw's work, the status of Cas-Tau as a *bona fide* moving group was debated in the literature on the basis of radial velocities (Petrie 1958) and large scatter in the color-Hβ relation (Crawford 1963). However, based on *Hipparcos* parallaxes, de Zeeuw et al. (1999) concluded that Cas-Tau is indeed a physical association that likely shares a common origin with α Per, though only a third of Blaauw's original sample were finally regarded as members.

Today, the low-mass membership of Cas-Tau remains essentially unknown. An X-ray survey in the direction of Taurus found evidence for a population of stars that are older and more widely distributed than the CTTS in the Taurus-Auriga star-formation complex (Walter et al. 1988). Those authors found that this distributed older population outnumbers the CTTS population by a factor of 10:1, and there are suggestions that this older population includes members of the Cas-Tau association (Hartmann et al. 1991; Walter & Boyd 1991). Assuming that all of Blaauw's original B-stars are indeed Cas-Tau members, Hartmann et al. (1991) argued based on expectations from the initial mass function that the projected surface density of members with masses $\gtrsim 0.8 M_{\odot}$ should be about 0.2 per square degree. In hindsight, that may be an overestimate given that the *Hipparcos* study found many of Blaauw's original sample are not likely to be members. Nevertheless, within the *K2* Campaign 13 field one might expect a couple dozen members in this mass range and an even larger number of lower-mass members. Since the area of Cas-Tau is so large on the sky, additional members might have plausibly been observed during other *K2* campaigns.

The precise age of Cas-Tau is not well known, in part due to our incomplete knowledge of the low-mass members. From the kinematics of the originally proposed members, Blaauw (1956) derived an expansion age for Cas-Tau in the range of 50–70 Myr. Due to the common kinematics between the associations, it is generally believed that Cas-Tau is younger than or coeval with α Per. Early examinations of the main sequence turnoff for α Per found ages of 50 Myr using models with no convective overshoot (Mermilliod 1981; Meynet et al. 1993). The age of α Per has since been refined using the lithium depletion boundary (LDB) technique, with estimates of 90 $\pm$ 10 Myr (Stauffer et al. 1999), 85 $\pm$ 10 Myr (Barrado y Navascués et al. 2004), and most recently 80 $\pm$ 11 $\pm$ 4 Myr (Soderblom et al. 2014). The LDB ages are broadly consistent with age estimates of 80 Myr from a color-magnitude diagram (CMD) of the lower main sequence (Prosser 1992), 80 Myr from an upper main sequence CMD age using models with moderate convective overshoot (Ventura et al. 1998), and 70 Myr from an H-R diagram of the upper main sequence (David & Hillenbrand 2015).

In the Appendix, we examine the main sequence turnoff for proposed members of Cas-Tau and derive a new estimate of the association age ($\tau_{\mathrm{Cas-Tau}} = 46 \pm 8$ Myr).

3.6. *Additional youth indicators*

Rotation: The photometric rotation period provides evidence of youth, as shown in Figure 10. For a star of its mass or color, EPIC 247267267 has a rotation period consistent with the slowly-rotating sequence of Pleiades members (Rebull et al. 2016), but about 3-4 d shorter than expected for members of Praesepe (Rebull et al. 2017) or the Hyades (Douglas et al. 2016). This is consistent with the picture that EPIC 247267267 is approaching or has only recently arrived on the ZAMS and has not had enough time to spin down via magnetic braking to a period reflective of older populations. Given the star's intrinsic $(B-V)$ color and its rotation period, we calculated the age of the star using the gyrochronology relations of both Barnes (2007), hereafter B07, and Mamajek & Hillenbrand (2008), hereafter MH08. Our gyrochronology ages take into account the uncertainties in the rotation period, $(B-V)$ color, as well as the published errors on the coefficients in the age-rotation relations (see Table 5). The B07 calibration produces an age that is roughly a factor of two younger than the age predicted from the MH08 relations ($\tau_{\mathrm{gyro,B07}} = 124$ Myr, compared to $\tau_{\mathrm{gyro,MH08}} = 262$ Myr). For completeness, we also investigated the Angus et al. (2015), hereafter A15, gyrochronology calibration and found that it closely reflects the MH08 predictions in the age and color range of interest here. To further investigate the differences and potential systematics in existing gyrochronology calibrations, we compared the relations to the intrinsic $(B-V)$ colors and rotation periods for members of the Pleiades and Praesepe clusters. The Pleiades photometry were gathered from Stauffer & Hartmann (1987) and Kamai et al. (2014), the Praesepe photometry from Upgren et al. (1979); Weis (1981); Stauffer (1982) and Mermilliod et al. (1990), and the rotation periods originate from Rebull et al. (2016, 2017). For this exercise we assumed $E(B-V) = 0.04$ for the Pleiades, and no reddening for Praesepe. Figure 10 shows that the B07 calibration most closely matches the Pleiades slowly-rotating sequence at the accepted age of the cluster, while the MH08 and A15 relations overpredict the age of the Pleiades. However, all calibrations predict a much younger age for Praesepe ($\sim$500 Myr) than the currently proposed value (790 Myr, Brandt & Huang 2015). A complete reassessment of gyrochronology calibrations using the voluminous rotation data now provided by *K2* is in order but outside the scope of this paper. We tentatively conclude that the younger gyrochronology age of EPIC 247267267 predicted by the B07 relations is likely to be more accurate given the ability of that calibration to reproduce the Pleiades data, but also note that gyrochronology is fundamentally a statistical age-dating method. We also note that gyrochronology is unreliable at ages younger than the Pleiades (because stars form with a range of rotation rates and low-mass stars at these young ages are still contracting and spinning up).

Chromospheric activity: EPIC 247267267 shows significant emission in the Ca II H&K lines (Fig. 13). The precise H&K values in our spectra are ambiguous due to the low SNR of ∼4 per pixel in the H&K orders. Nevertheless, we report our measured $\log R'_{HK}$ and the S-index with large uncertainties in Table 5. Our best estimate of $\log R'_{HK}$ is just barely outside the high-activity range where the activity-age relations of Mamajek & Hillenbrand (2008) were calibrated. Regardless, we estimated an activity age by modeling $\log R'_{HK}$ as a normal distribution with the values specified in Table 5 and imposing a cutoff upwards of -4.0. From this analysis we estimated the activity age to be <435 Myr at 68% confidence.

Near-UV emission: While there is no X-ray detection of EPIC 247267267, the star was detected at near-UV wavelengths with *GALEX*. Young, low-mass stars have been shown to exhibit significant emission above photospheric levels in the near-UV (NUV, 1750–2750 Å) and far-UV (FUV, 1350–1750 Å) *GALEX* passbands (Findeisen & Hillenbrand 2010; Shkolnik et al. 2011; Rodriguez et al. 2011, 2013; Kraus et al. 2014). Specifically, Shkolnik et al. (2011) found that young (<300 Myr) late-K and M-dwarfs generally show fractional flux densities of $F_{\rm NUV}/F_{\rm J} > 10^{-4}$ while older stars tend to fall below this threshold. EPIC 247267267 has a fractional flux density of $F_{\rm NUV}/F_{\rm J} = 1.1 \times 10^{-4}$. Using near-UV photometry from *GALEX* and near-IR photometry from 2MASS, we estimated the stellar age based on the (NUV-J) and ($J-K$) colors and the empirical relations presented in Findeisen et al. (2011). Empirical isochrones from that work are shown in Figure 11, along with comparisons to other known young stellar populations. While there is a large amount of scatter in this color-color diagram, particularly

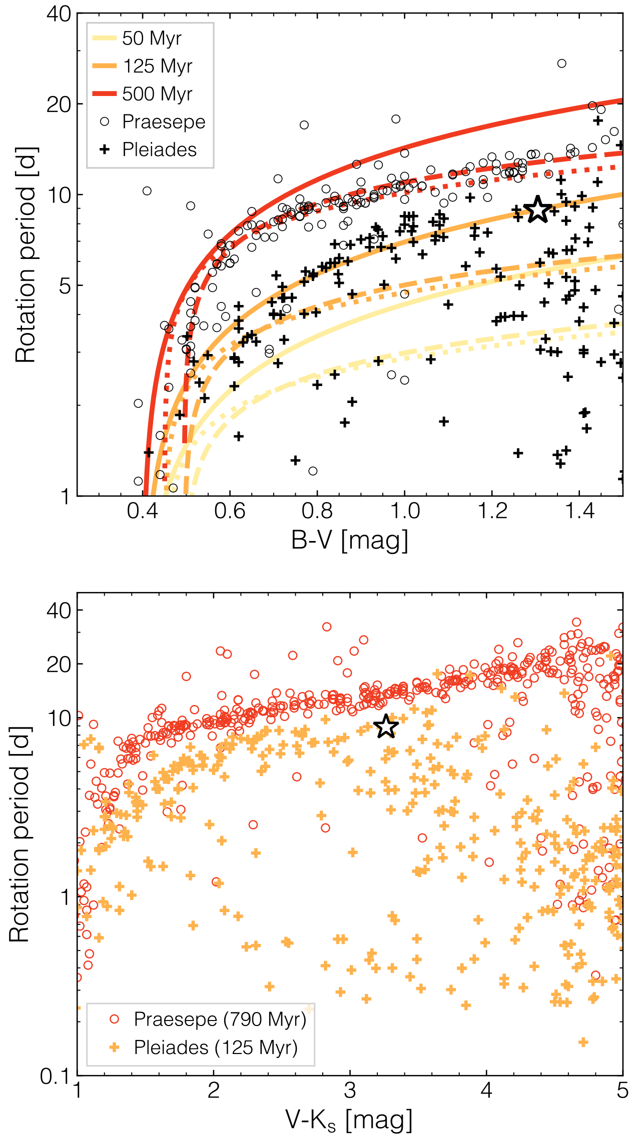

Figure 10. *Top:* Gyrochrones in the period versus $(B-V)$ plane. The solid, dashed, and dotted lines show gyrochrones predicted from Barnes (2007), Mamajek & Hillenbrand (2008), and Angus et al. (2015), respectively. *Bottom:* Rotation periods versus $(V-K_s)$ color for Praesepe (red) and Pleiades (orange) members. In both figures the cluster rotation periods are taken from Rebull et al. (2016, 2017) and the white star indicates EPIC 247267267.

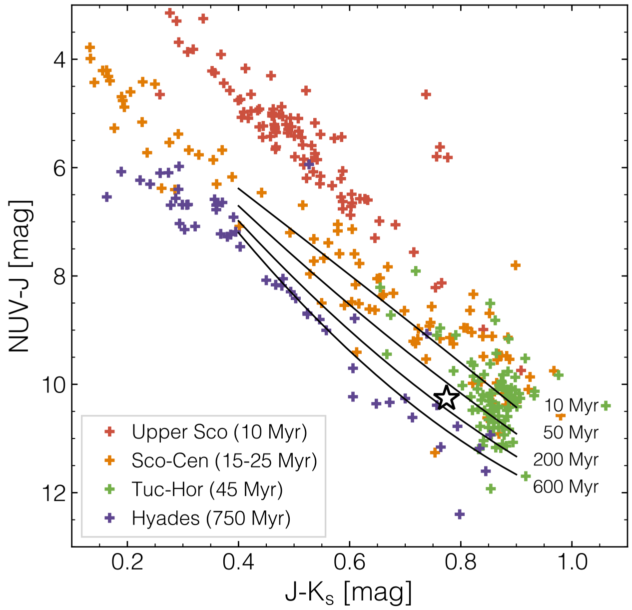

Figure 11. NUV and NIR color-color diagram showing empirical isochrones of Findeisen et al. (2011) and members of young stellar populations. EPIC 247267267 is indicated by the white star.

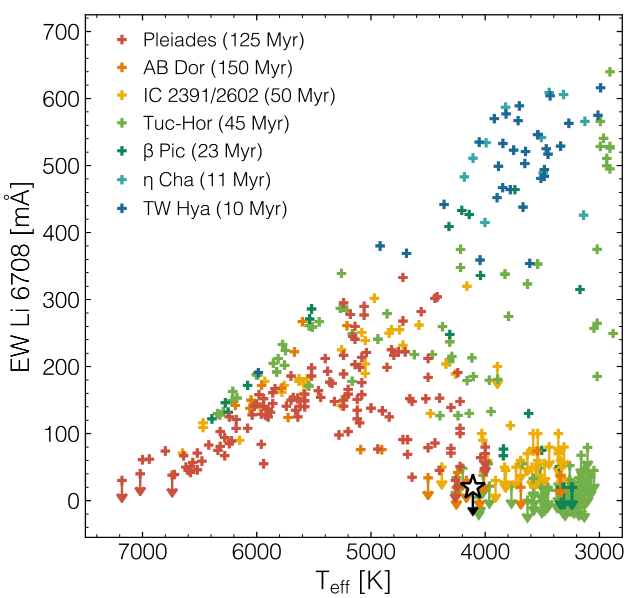

Figure 12. Li I 6708 Å equivalent width versus $T_{\rm eff}$ for members of Pleiades (Soderblom et al. 1993), IC 2391/2602 (Randich et al. 2001), and young moving groups (Mentuch et al. 2008; Kraus et al. 2014). EPIC 247267267 is indicated by the white star.

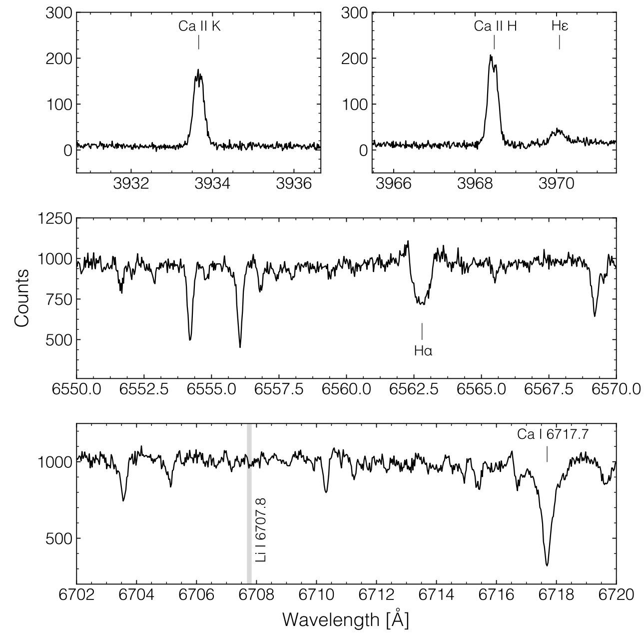

Figure 13. Sections of the HIRES spectra used as age diagnostics. Chromospheric emission in the Ca II H&K lines is clearly detected (top panels) as well as Hϵ emission. The Hα profile shows absorption with emission filling in the wings of the line (middle panel), reminiscent of slowly-rotating late-type stars in the Pleiades and some G-type stars in α Per. The Li I 6708 Å absorption line is clearly not present, which is broadly consistent with slowly-rotating mid-K dwarfs in the Pleiades and stars of similar $T_{\rm eff}$ in moving groups with ages >20–50 Myr.

for later-type stars, there is a clear qualitative trend of declining NUV flux for older stars. Proposed Upper Sco and Sco-Cen members were selected from the Young Stellar Object Corral (YSOC), Tuc-Hor members from Kraus et al. (2014), and Hyades members from Perryman et al. (1998). The photometry were dereddened using the extinction coefficients of Yuan et al. (2013) and assuming $A(V) = 0.7$ mag for Upper Sco and $A(V) = 0.16$ mag for Sco-Cen.

Spectroscopic indicators: EPIC 247267267 exhibits a weak Hα absorption feature with emission filling in the wings of the line (Fig. 13). This is consistent with the model line profiles produced for weakly active dwarf stars in Cram

& Mullan (1979). Hα profiles of this type have been observed for some of the most slowly-rotating late-type stars in the Pleiades, e.g. the M0 member SK 17 (Stauffer et al. 2016), some G-type members of α Per (Stauffer et al. 1989), as well as the M-type Praesepe planet host K2-95 (Obermeier et al. 2016). At the age of the Pleiades, there is a transition at mid-K spectral types where nearly all earlier type stars show Hα in absorption and at later types nearly all show the line in emission (Stauffer & Hartmann 1987). In α Per, this transition occurs approximately at a spectral type of K6 (Prosser 1992). Thus, the lack of strong Hα emission in EPIC 247267267 is at least consistent with expectations of other stars of a similar mass and age, and in fact some members of Sco-Cen ($\lesssim$20 Myr) with a similar effective temperature also show Hα in absorption (Pecaut & Mamajek 2016). Similar to other late-type stars in young moving groups, EPIC 247267267 exhibits weak emission in other Balmer lines, including Hϵ (seen in Fig. 13), Hζ, and Hη.

We do not detect Li I 6708 Å within the spectrum of EPIC 247267267. From the HIRES spectrum, we estimated an upper limit to EW(Li) of <20 mÅ. This is not unexpected given that some late-K dwarfs with ages $\gtrsim$20 Myr are observed to show significant lithium depletion (see Fig. 12). Depletion of lithium below detectable levels has been observed in mid- to late-K members of IC 2391 and 2602 (~50 Myr Barrado y Navascués et al. 2004; Dobbie et al. 2010), AB Dor (149^{+51}_{-19} Myr, Bell et al. 2015), and Tuc-Hor (45 ± 4 Myr, Bell et al. 2015). In the 125 Myr-old Pleiades, Soderblom et al. (1993) found that mid- to late-K stars exhibit a wide range of Li I 6708 Å equivalent widths, of approximately 20–300 mÅ. Furthermore, at the age of the Pleiades, some stars of a similar mass or color to EPIC 247267267 have yet to spin down. Bouvier et al. (2017) have found that more slowly rotating Pleiads in a given mass range also tend to have weaker lithium absorption. Considered together, the rotation and lithium properties of EPIC 247267267 are consistent with Pleiades-aged or younger mid- to late-K dwarfs. In Figure 12 we show the distribution of Li I 6708 Å equivalent width measurements as a function of $T_{\rm eff}$ for members of young moving groups and clusters.

H-R diagram and stellar density: Since the star is on or very nearly on the main sequence, where evolution is slow for these low-mass stars, isochronal age estimates carry large uncertainties. Nevertheless, as we estimated the mass from interpolation between the PARSECv1.2S models (Bressan et al. 2012; Chen et al. 2014), we also estimated the age in the theoretical H-R diagram using the spectroscopic $T_{\rm eff}$ and the Stefan-Boltzmann luminosity. Because EPIC 247267267 is expected to be near or on the main sequence, the mean stellar density from the transit fits is also not particularly useful for constraining the stellar age, in part due to the fact that the impact parameter is not tightly constrained by the *K2* data. Regardless, we also estimated the stellar age from the directly-determined stellar density distribution (from the circular orbit transit fit discussed in § 3.1), a normal distribution in $T_{\rm eff}$, and the PARSECv1.2S models. Though not very precise, the isochronal age estimates (through the H-R diagram or the mean stellar density) do provide a consistent lower limit of 30–40 Myr. From the lack of lithium, it is very unlikely the star is as young as the β Pic moving group (23 ± 3 Myr, Mamajek & Bell 2014). However, with respect to the lithium levels in other young low-mass stars, ages corresponding to the moving groups Tuc-Hor (Kraus et al. 2014), AB Dor (Mentuch et al. 2008) or the clusters IC 2391/2602 (Randich et al. 2001) are plausible.

In Table 5, we report several determinations of the host star age derived through the differ-

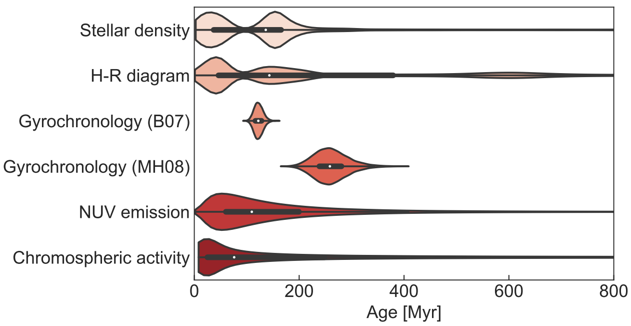

Figure 14. Violin plot demonstrating the kernel density estimates for stellar age distributions resulting from different age-dating methods discussed in § 3.6.

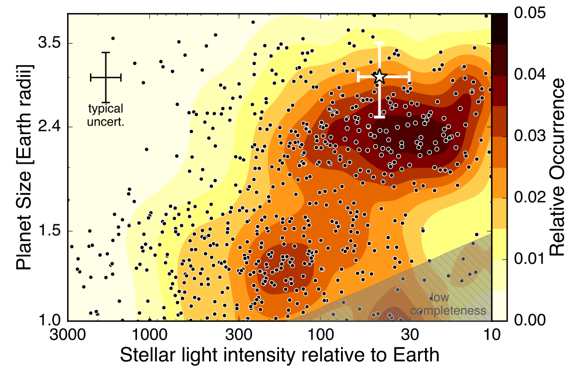

Figure 15. The distribution of small transiting planets from the California-Kepler Survey sample (Fulton et al. 2017) in the plane of planet radius and insolation flux. EPIC 247267267 b is indicated by the white star.

ent methods described above. We also show the resulting age distributions from these methods and Monte Carlo error propagation in the various input parameters in Figure 14. While the age indicators discussed above are statistical in nature, they present a consistent picture of a star that is (1) on or very nearly on the ZAMS, (2) unlikely to be as young as the youngest moving groups in the solar neighborhood, and (3) almost certainly younger than the Hyades or Praesepe. The H-R diagram and stellar density analyses are not precise age indicators in this case, but they at least present consistent lower limits to the age of >30–40 Myr (at 68% confidence) or >10 Myr (at 95% confidence). Due to the large uncertainty in $\log R'_{HK}$, our chromospheric activity age distributions also have long tails to unrealistically old ages, but we can still derive lower limits of >20 Myr (at 68% confidence) or >10 Myr (at 95% confidence). The NUV emission levels suggest an age of 45–270 Myr at 68% confidence or 20–640 Myr at 95% confidence, though we note the Findeisen et al. (2011) study calibrated the NUV/NIR age relations using cluster ages that have since been revised. Our tightest age constraints result from the gyrochronology relations, which suggest 95% confidence intervals in age of 100–160 Myr or 200–350 Myr depending on the preferred calibration.

Considered collectively, these independent age estimates are consistent with a stellar age of $\tau_* = 150^{+350}_{-100}$ Myr (corresponding to the median and 68% confidence interval of the age distribution resulting from combining each of the different methods and weighting them equally). The long tail towards older ages is due to the H-R diagram and stellar density analyses as well as the uncertain $\log R'_{HK}$ value. However, based on the stellar kinematics, we suggest the star is a member of the Cas-Tau association. In the Appendix, we derive a new main-sequence turnoff age for the association, $\tau_{\mathrm{Cas-Tau}} = 46 \pm 8$ Myr. While this age is on the younger end of the interval quoted above, we note again that gyrochronology in particular is not reliable at such young ages. The upcoming second *Gaia* data release will resolve the issue of whether Cas-Tau is a real association, and whether EPIC 247267267 belongs to that association or not.

4. DISCUSSION

At first glance, EPIC 247267267 b appears fairly typical when compared with other transiting sub-Neptunes receiving similar incident flux. That is, EPIC 247267267 b does not reside in a region of particularly low occur-

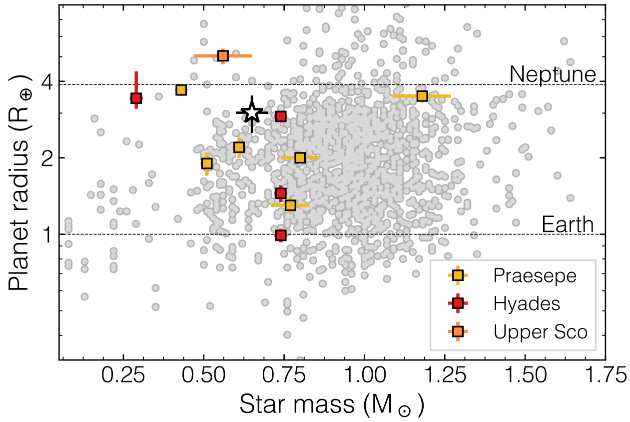

Figure 16. The distribution of small transiting planets (with orbital periods ≤30 d) from the NASA Exoplanet Archive (Akeson et al. 2013) in the plane of planet radius and host star mass. Other planets transiting stars in clusters or associations are highlighted as colored squares. EPIC 247267267 b is indicated by the white star. While not in a region that is totally unpopulated, EPIC 247267267 b is on the larger end of known, close-in sub-Neptunes around stars of a similar mass.

rence in the plane of planet radius and insolation flux (Fulton et al. 2017), as shown in Figure 15. Thus, at least some young (<1 Gyr) sub-Neptunes superficially resemble the statistically older population uncovered by *Kepler*. This much was known for slightly more mature planets in the ≃800 Myr-old Hyades and Praesepe clusters, and we can now extend this conclusion to younger ages.

However, the stars in the California-Kepler Survey are all more massive than EPIC 247267267 (Petigura et al. 2017). When compared to other small transiting planets around low-mass stars, EPIC 247267267 b does appear to reside in the large-radius tail of the size distribution for close-in sub-Neptunes. This is apparent in both the host star mass versus planet radius plane (Figure 16) as well as the planet radius versus insolation flux plane for low-mass stars (see Fig. 10 of Mann et al. 2017b). In this case, it seems clear the *K2* photometry of EPIC 247267267 are sensitive to planets much smaller than EPIC 247267267 b, though injection and recovery tests would be needed to quantify how sensitive the data are. In any event, while we can not be sure that the relatively large size of EPIC 247267267 b is due to its young age, it at least does not appear to be merely a consequence of observational bias.

The radius of EPIC 247267267 b is not particularly well-constrained, although the uncertainty is not much larger than the typical radius error for a planet in the California-Kepler Survey. The planet radius uncertainty is dominated by the stellar radius uncertainty (16%), with a minor contribution from the uncertainty in the radius ratio (about 5%). A trigonometric parallax from *Gaia* DR2 should help better constrain the stellar luminosity and radius. Better constraints on the impact parameter and thus radius ratio might be achieved by observing transits with *Spitzer*, where stellar activity is low and limb-darkening is negligible. Such observations should also lead to a tighter constraint on the mean stellar density, which in turn can help to better constrain the age of the system.

Ultimately, a comparison between the typical densities of young and old planets may be more elucidating than simply comparing radii. This requires a determination of the planet's mass. From the planet radius distribution, we calculated a predicted mass for EPIC 247267267 b of $9.2^{+7.9}_{-4.4} M_\oplus$ using the `forecaster`[2] tool in PYTHON, which is based on the Chen & Kipping (2017a) mass-radius relations for exoplanets. For this range of plausible planet masses and the stellar mass we adopt, we calculated an expected Doppler semi-amplitude of 2.4–8.6 m s^{-1}. Notably, existing exoplanet mass-radius relations are calibrated using field-aged planets. If sub-Neptunes as young as EPIC 247267267 b are less dense at

[2] https://github.com/davidkipping/forecaster

early times, then the true Doppler amplitude may be on the lower end of the range quoted. While the expected Doppler amplitude is within reach of current precision RV instruments, the relatively high stellar activity will likely present challenges. Given the measured chromospheric activity level for EPIC 247267267, it is likely the RV jitter is greater than 30 m s^{-1} and possibly larger than 100 m s^{-1} (Hillenbrand et al. 2015). The RV jitter may also be approximated from the amplitude of photometric variability and $v \sin i_*$, from the equation $\sigma_{\rm RV} = {\rm rms}_{K2} \times v \sin i_*$, which yields 33 m s^{-1}, considerably larger than the expected signal from the planet. Since the star is brighter and activity should be lower at infrared wavelengths, it would be advantageous to measure the planet's mass with an IR precision spectrograph such as the PARVI instrument planned for Palomar Observatory or one of many other spectrographs in operation or development (Plavchan et al. 2015).

Interestingly, no transiting planets have yet been confirmed in the Pleiades, despite systematic searches within the *K2* data of ∼1000 members (Rizzuto et al. 2017; Gaidos et al. 2017). A single candidate was reported by Rizzuto et al. (2017), but the planet has not yet been validated and the probability of Pleiades membership was estimated to be 62%. By comparison, six confirmed transiting planet hosts and one candidate have been reported in Praesepe (Mann et al. 2017b; Libralato et al. 2016; Obermeier et al. 2016; Pepper et al. 2017), a cluster with a distance and metallicity not much different from the Pleiades and for which a similar number of members were observed by *K2*. In the Hyades, four transiting planets around two hosts have been found in a search of <200 members (Mann et al. 2016b, 2017a; Ciardi et al. 2017; Livingston et al. 2017; David et al. 2016b). An important difference between the clusters is that at the age of the Pleiades most members are spinning as rapidly as they ever will, while Praesepe and Hyades stars have spun down considerably and are thus more amenable to transit searches. It is also possible that the Pleiades members show enhanced photometric activity (in the form of larger and more frequent flares, larger variability amplitudes, and/or more rapidly evolving spot patterns), making the removal of these trends more difficult. It may be tempting to ascribe the lack of planets in the Pleiades (to this point) to some physical mechanism such as ongoing orbital migration or differences in the cluster environments. However, with an age unlikely to be much older than the Pleiades, the case of EPIC 247267267 b highlights the importance of taking a holistic approach towards the comparison of planet occurrence rates at young and old ages.

 This research was carried out at the Jet Propulsion Laboratory, California Institute of Technology, under a contract with the National Aeronautics and Space Administration. TJD and EEM acknowledge support from the Jet Propulsion Laboratory Exoplanetary Science Initiative. MB acknowledges support from the North Carolina Space Grant Consortium. This work was performed in part under contract with the California Institute of Technology (Caltech)/Jet Propulsion Laboratory (JPL) funded by NASA through the Sagan Fellowship Program executed by the NASA Exoplanet Science Institute. This paper includes data collected by the Kepler mission. Funding for the Kepler mission is provided by the NASA Science Mission directorate. Some of the data presented in this paper were obtained from the Mikulski Archive for Space Telescopes (MAST). STScI is operated by the Association of Universities for Research in Astronomy, Inc., under NASA contract NAS5-26555. Support for MAST for non-HST data is provided by the NASA Office of Space Science via grant NNX09AF08G and by other grants and contracts. Some of the data presented herein were obtained at the W. M. Keck Observatory, which is operated as a scientific partnership among the California Institute of Technology, the University of California and the National Aeronautics and Space Administration. The Observatory was made possible by the generous financial support of the W. M. Keck Foundation. The authors wish to recognize and acknowledge the very significant cultural role and reverence that the summit of Maunakea has always had within the indigenous Hawaiian community. We are most fortunate to have the opportunity to conduct observations from this mountain. This research has made use of the VizieR catalogue access tool, CDS, Strasbourg, France. The original description of the VizieR service was published in A&AS 143, 23. The Pan-STARRS1 Surveys (PS1) and the PS1 public science archive have been made possible through contributions by the Institute for Astronomy, the University of Hawaii, the Pan-STARRS Project Office, the Max-Planck Society and its participating institutes, the Max Planck Institute for Astronomy, Heidelberg and the Max Planck Institute for Extraterrestrial Physics, Garching, The Johns Hopkins University, Durham University, the University of Edinburgh, the Queen's University Belfast, the Harvard-Smithsonian Center for Astrophysics, the Las Cumbres Observatory Global Telescope Network Incorporated, the National Central University of Taiwan, the Space Telescope Science Institute, the National Aeronautics and Space Administration under Grant No. NNX08AR22G issued through the Planetary Science Division of the NASA Science Mission Directorate, the National Science Foundation Grant No. AST-1238877, the University of Maryland, Eotvos Lorand University (ELTE), the Los Alamos National Laboratory, and the Gordon and Betty Moore Foundation. This work has made use of data from the European Space Agency (ESA) mission *Gaia* (`https://www.cosmos.esa.int/gaia`), processed by the *Gaia* Data Processing and Analysis Consortium (DPAC, `https://www.cosmos.esa.int/web/gaia/dpac/consortium`). Funding for the DPAC has been provided by national institutions, in particular the institutions participating in the *Gaia* Multilateral Agreement.

Facilities: FLWO:1.5m (TRES), Keck:I (HIRES), Keck:II (NIRC2), Kepler, PS1, Shane (ShARCS)

Software: batman (Kreidberg 2015), emcee (Foreman-Mackey et al. 2013), forecaster (Chen & Kipping 2017b), k2sc (Aigrain et al. 2016), k2sff (Vanderburg & Johnson 2014), radvel (Fulton et al. 2018), vespa (Morton 2015)

APPENDIX

A. A TURNOFF AGE FOR CAS-TAU

To our knowledge, the only determination of a turnoff age for Cas-Tau is the estimate of 20-30 Myr from de Zeeuw & Brand (1985). Motivated by our suggestion that the planet host EPIC 247267267 belongs to the association, we derive a new turnoff age here. We began with the list of 83 B- and A-type members proposed by de Zeeuw et al. (1999). For each of the proposed members, we gathered trigonometric parallaxes from the *Gaia* TGAS catalog (Gaia Collaboration et al. 2016a,b) when available and from the Extended *Hipparcos* compilation otherwise (XHIP, Anderson & Francis 2012). For each star we then gathered UBV photometry from Mermilliod (2006) and $uvby\beta$ photometry from Paunzen (2015). Of the 83 proposed members, 19 stars were missing both UBV and $uvby\beta$

photometry from the aforementioned compilations, while 5 stars lacked only the UBV data and 11 stars lacked only the $uvby\beta$ data. Nearly all of the stars missing photometry have spectral types of B8 or later, and given that we determine the main-sequence turnoff to be around spectral type B2 for Cas-Tau, these stars contribute little information to the turnoff age anyhow. Our motivation for including both UBV and $uvby\beta$ photometry was for the purposes of consistency checks. We ultimately derived the turnoff age from UBV photometry, so stars missing those data were excluded from our analysis, and any star that lacked both UBV and $uvby\beta$ photometry was not included in our various consistency checks described below. To guide our analysis, we additionally gathered spectral types from Skiff (2014), $v \sin i$ measurements and multiplicity information from Abt et al. (2002). For each star we also performed literature searches for further information on multiplicity and to vet for eclipsing binaries (EBs).

Many of the proposed members are reddened. We determined the amount of reddening for each star using the UBV photometry and the revised Q-method presented in Pecaut & Mamajek (2013). For those stars with $uvby\beta$ photometry we used the iterative dereddening scheme of Shobbrook (1983) to determine an independent value for the extinction. Among the stars with both sets of photometry, we found the $A(V)$ values derived from the Q-method and the $uvby\beta$ iterative method to be well-described by a one-to-one relation with a scatter of 0.066 mag. From an empirical relation between $(b-y)_0$ and $(B-V)_0$ for B-type stars (Crawford 1978), we also compared the intrinsic $(B-V)$ colors from the two different dereddening methods and found these to be in good agreement with a scatter of 0.01 mag. We ultimately used the intrinsic colors and $A(V)$ values from the UBV photometry, but we adopted 0.01 mag as the uncertainty in $(B-V)_0$ for our turnoff age analysis to account for the different estimates provided by the $uvby\beta$ photometry.

Using the intrinsic $(B-V)_0$ colors and M_V magnitudes calculated from the V-band photometry and trigonometric parallaxes, we then proceeded to estimate the turnoff age from comparison with the PARSECv1.2S evolutionary models (Bressan et al. 2012). The uncertainties in the M_V magnitudes were determined from Monte Carlo error estimation, accounting for the uncertainties in V magnitudes and the parallaxes. For high-mass stars such as those considered here, the PARSECv1.2S models are transformed into the observational system through the use of Castelli & Kurucz (2004) model atmospheres, Bessell (1990) $UBVRI$ passbands, and the zero-points presented in Maíz Apellániz (2006). We used models with a solar metallicity of Z=0.0152 (Caffau et al. 2011) for this analysis.

From the color-magnitude diagram, it is apparent that there is a significant amount of scatter around the turnoff. It is possible that there are interlopers in the de Zeeuw et al. (1999) sample, so in an attempt to address this issue we considered only stars with membership probabilities $\geq$90%, where the probability values originate from those authors. We additionally excluded two high-probability members since these are emission line stars. These stars are HD 9709 (HIP 7457), a B7IV/Vne shell star, and ϕ Per (HIP 8068), a B1.5V:e shell star and double-lined spectroscopic binary. Furthermore, several of the proposed members are eclipsing binaries. These stars are 1 Per (HIP 8704), τ Ari (HIP 15627), 17 Aur (HIP 24740), and 15 Cam (HIP 24836).[3] We ultimately excluded 1 Per and 17 Aur on the basis of large eclipse depths (>0.3 mag) and included the other two systems given their more moderate eclipse depths (Avvakumova et al. 2013). In the course of our analysis, we also found that two of the proposed members are surrounded by reflection nebulae (HD 26676 and HD 17443).

[3] μ Eri (HIP 22109) is also listed as an EB in SIMBAD, but we did not find published evidence in support of this interpretation in the literature. This star was excluded from the age analysis anyhow on the basis of its low membership probability.

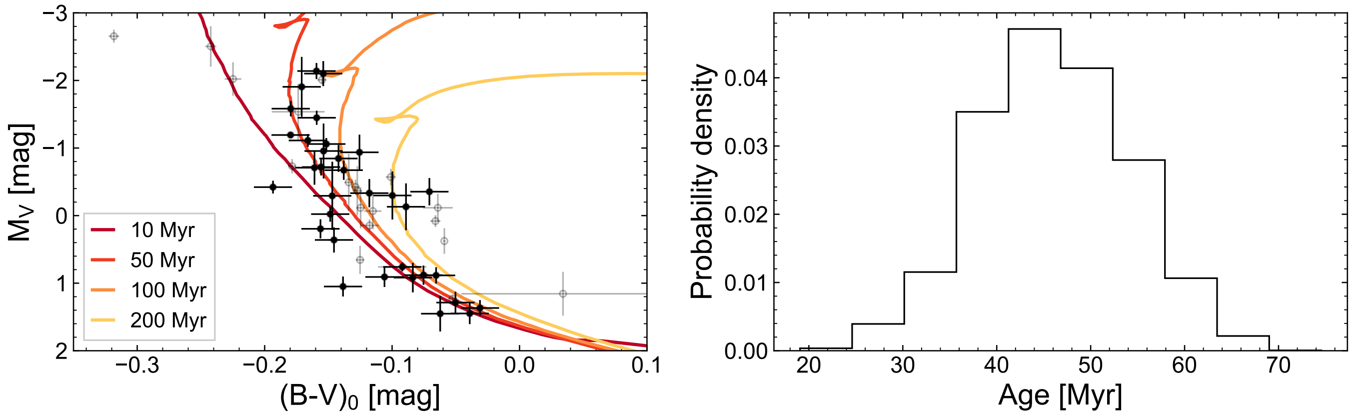

Figure 17. *Left:* Color-magnitude diagram for proposed members of Cas-Tau. Black points are the high probability members we used to determine the turnoff age, while the grey points show members that were excluded for the reasons described in the text. Isochrones from the PARSECv1.2S models are indicated by the colored curves. The grey lines indicate the reddened colors of each star. *Right:* Histogram of turnoff ages resulting from 10^4 Monte Carlo simulations.

Despite the additional extinction, these stars do not appear to be obvious outliers in the CMD and were included in the age analysis.

Using a fine grid of isochrones ($\Delta \log \tau = 0.0025$ dex) with ages between 10^6 and 10^9 yr we fit an isochrone of each age to the data and evaluated χ^2. We determined the uncertainty on the turnoff age from 10^4 Monte Carlo simulations in which a new $\chi^2_{\rm min}$ age was calculated from perturbed M_V and $(B-V)_0$ values for each star. In this analysis the perturbed M_V and $(B-V)_0$ values were drawn from normal distributions in accordance with that star's individual errors. For those stars missing V magnitude error estimates, we assumed an error of 0.01 mag. Ultimately, we found a turnoff age of $\tau_{\rm Cas-Tau} = 46 \pm 8$ Myr, where the value and uncertainty are the median and standard deviation, respectively, of the distribution of ages from the Monte Carlo simulations. This age is in good agreement with the original kinematic estimate of 50–70 Myr from Blaauw (1956), and somewhat younger than the lithium depletion boundary age ($80 \pm 11 \pm 4$ Myr, Soderblom et al. 2014) and turnoff ages derived for the α Per cluster (80 Myr, Ventura et al. 1998).

Table 6. Cas-Tau members.

Name	HIP	Prob. (%)	SpT	ϖ (mas)	V (mag)	M_V (mag)	$B-V$ (mag)	$U-B$ (mag)	$(B-V)_0$ (mag)	$(U-B)_0$ (mag)	$E(B-V)$ (mag)	A_V (mag)
HD 1976	1921	100	B5IV	3.26 ± 0.63	5.571 ± 0.015	-1.912 ± 0.473	-0.122 ± 0.009	-0.603 ± 0.010	-0.171 ± 0.004	-0.637 ± 0.015	0.049 ± 0.012	0.159 ± 0.038
HD 2626	2377	100	B9IIIn	4.24 ± 0.5	5.942 ± 0.004	-0.913 ± 0.261	0.006 ± 0.007	-0.359 ± 0.003	-0.126 ± 0.002	-0.453 ± 0.007	0.132 ± 0.008	0.431 ± 0.027
13 Cas	2474	98	B6V	4.29 ± 0.28	6.170	-0.676 ± 0.146	-0.100	-0.480	-0.138 ± 0.003	-0.506 ± 0.015	0.039 ± 0.012	0.127 ± 0.039
λ Cas	2505	80	B8Vnn	8.64 ± 0.43	4.749 ± 0.054	-0.572 ± 0.118	-0.101 ± 0.004	-0.340 ± 0.020	-0.101 ± 0.004	-0.340 ± 0.020	0.000	0.000
HD 2974	2647	97	B8:	4.04 ± 0.4	7.897 ± 0.009	0.923 ± 0.217	-0.007 ± 0.005	-0.210	-0.084 ± 0.003	-0.266 ± 0.013	0.077 ± 0.007	0.251 ± 0.021
HD 3291	2866	97	B9	3.64 ± 0.45	...	...	...	...	...	...	...	...
omi Cas	3504	99	B5III	4.64 ± 0.38	4.573 ± 0.046	-2.107 ± 0.187	-0.069 ± 0.009	-0.512 ± 0.016	-0.154 ± 0.005	-0.571 ± 0.021	0.084 ± 0.012	0.275 ± 0.039
HD 5409	4437	99	B9V	3.2 ± 0.54	7.852 ± 0.015	0.326 ± 0.398	0.038 ± 0.022	...	...	...	...	...
HR 302	5062	100	B3V	2.48 ± 0.45	6.528 ± 0.013	-1.544 ± 0.419	-0.081 ± 0.010	-0.579 ± 0.061	-0.173 ± 0.020	-0.642 ± 0.074	0.092 ± 0.023	0.299 ± 0.075
HR 342	5566	51	B9.5V	8.06 ± 0.32	5.551 ± 0.011	0.083 ± 0.087	-0.066 ± 0.004	-0.135 ± 0.158	-0.066 ± 0.004	-0.135 ± 0.158	0.000	0.000
HD 7349	5813	97		3.5 ± 0.64	...	...	...	...	...	...	...	...
HD 8346	6480	99	A0V	7.2 ± 0.39	...	...	...	...	...	...	...	...
HD 9709	7457	98	B7IV/Vne[a]	3.13 ± 0.58	7.070	-0.513 ± 0.416	-0.050	-0.430	-0.134 ± 0.003	-0.490 ± 0.015	0.084 ± 0.012	0.276 ± 0.040
HD 10404	7988	88	B8IV	3.54 ± 0.52	...	...	...	...	...	...	...	...
ϕ Per	8068	100	B1.5V:e[a]	4.54 ± 0.2	4.062 ± 0.012	-2.655 ± 0.092	-0.042 ± 0.007	-0.935 ± 0.012	-0.318 ± 0.004	-1.131 ± 0.015	0.276 ± 0.009	0.891 ± 0.030
HD 10577	8108	100	B9V	3.76 ± 0.58	7.020	-0.133 ± 0.349	0.020	-0.210	-0.089 ± 0.003	-0.290 ± 0.015	0.109 ± 0.012	0.357 ± 0.040
4 Ari	8387	54	B9.5V	11.85 ± 0.25	5.860	1.228 ± 0.046	-0.037 ± 0.005	-0.133 ± 0.009	-0.053 ± 0.003	-0.144 ± 0.012	0.016 ± 0.007	0.051 ± 0.023
HD 11104	8551	100	B8IV/V	2.23 ± 0.61	...	...	...	...	...	...	...	...
1 Per	8704	98	B2V	2.52 ± 0.33	5.508 ± 0.073	-2.512 ± 0.308	-0.179 ± 0.008	-0.834 ± 0.009	-0.242 ± 0.004	-0.880 ± 0.014	0.063 ± 0.011	0.204 ± 0.034
ϵ Cas	8886	93	B3V	7.92 ± 0.43	3.370 ± 0.009	-2.134 ± 0.117	-0.155 ± 0.007	-0.591 ± 0.014	-0.159 ± 0.005	-0.592 ± 0.018	0.004 ± 0.009	0.014 ± 0.031
HD 12518	9656	100	B9IV	7.09 ± 0.48	6.660	0.910 ± 0.145	-0.030	-0.310	-0.106 ± 0.003	-0.365 ± 0.015	0.076 ± 0.012	0.247 ± 0.040
HD 12844	9890	98		4.7 ± 0.41	...	...	...	...	...	...	...	...
HR 679	10924	99	B5V	4.1 ± 0.37	6.100	-0.836 ± 0.194	-0.080	-0.480	-0.142 ± 0.003	-0.524 ± 0.014	0.062 ± 0.012	0.203 ± 0.040
63 And	10944	89	B9VpSi	8.31 ± 0.34	5.550	0.145 ± 0.092	-0.094 ± 0.029	-0.401 ± 0.017	-0.118 ± 0.007	-0.418 ± 0.031	0.024 ± 0.035	0.079 ± 0.113
BD+67 195	10974	95	B2	4.22 ± 0.26	...	...	...	...	...	...	...	...
HD 14795	11295	99	B5V	4.73 ± 0.32	7.680	1.044 ± 0.145	0.000	-0.410	-0.139 ± 0.003	-0.509 ± 0.015	0.139 ± 0.012	0.453 ± 0.040
HR 760	12218	100	B5V	4.25 ± 0.5	...	...	-0.120 ± 0.000	-0.483 ± 0.005	-0.135 ± 0.002	-0.493 ± 0.010	0.015 ± 0.012	0.048 ± 0.039
HD 16485	12453	99	B9V	3.35 ± 0.39	...	...	...	...	...	...	...	...
HD 16449	12477	100	B9V	3.41 ± 0.39	...	...	...	...	...	...	...	...
BD+65 291	13003	74	B8	5.42 ± 0.25	...	...	...	...	...	...	...	...
HD 17359	13124	93	A0Vs	5.29 ± 0.77	7.563 ± 0.002	1.155 ± 0.321	0.037 ± 0.012	0.065 ± 0.106	0.033 ± 0.077	0.084 ± 0.183	0.004 ± 0.079	0.012 ± 0.263
sig Ari	13327	86	B7V	6.6 ± 0.32	5.480	-0.427 ± 0.107	-0.089 ± 0.002	-0.439 ± 0.012	-0.129 ± 0.003	-0.467 ± 0.014	0.040 ± 0.004	0.129 ± 0.013
HD 17443	13330	100	B9V	3.49 ± 0.25	8.740 ± 0.000	1.448 ± 0.158	0.302 ± 0.010	0.145 ± 0.019	-0.039 ± 0.008	-0.098 ± 0.028	0.341 ± 0.015	1.126 ± 0.050
HR 950	14887	100	B4V	4.99 ± 0.4	...	...	-0.090	-0.570	-0.168 ± 0.004	-0.624 ± 0.015	0.078 ± 0.013	0.253 ± 0.041
HD 19981	15065	75	B9IV	5.86 ± 0.8	...	...	...	...	...	...	...	...
HD 20336	15520	87	B2IV:e	4.28 ± 0.48	4.835 ± 0.028	-2.027 ± 0.247	-0.152 ± 0.014	-0.771 ± 0.013	-0.225 ± 0.006	-0.823 ± 0.020	0.073 ± 0.018	0.235 ± 0.059
HD 20510	15531	98	B9V	5.85 ± 0.38	7.050	0.885 ± 0.142	0.050	-0.140	-0.075 ± 0.004	-0.231 ± 0.015	0.125 ± 0.013	0.411 ± 0.042

Table 6 continued

Table 6 *(continued)*

Name	HIP	Prob.	SpT	ϖ	V	M_V	$B-V$	$U-B$	$(B-V)_0$	$(U-B)_0$	$E(B-V)$	A_V
		(%)		(mas)	(mag)	(mag)	(mag)	(mag)	(mag)	(mag)	(mag)	(mag)
τ Ari	15627	100	B5III	6.41 ± 0.73	5.271 ± 0.012	-0.708 ± 0.251	-0.067 ± 0.008	-0.531 ± 0.048	-0.161 ± 0.016	-0.597 ± 0.061	0.094 ± 0.018	0.306 ± 0.060
u Tau	17563	80	B3V	6.11 ± 0.29	5.341 ± 0.020	-0.730 ± 0.103	-0.112 ± 0.004	-0.618 ± 0.008	-0.179 ± 0.003	-0.665 ± 0.011	0.067 ± 0.006	0.216 ± 0.018
HD 23477	17681	98		7.26 ± 0.39	7.066	1.367 ± 0.113	0.010	-0.046	-0.031 ± 0.006	-0.071 ± 0.018	0.041 ± 0.014	0.134 ± 0.046
HR 1147	17707	93	B9Vnn	9.07 ± 0.5	6.100	0.885 ± 0.125	-0.022 ± 0.011	-0.160	-0.066 ± 0.004	-0.193 ± 0.017	0.044 ± 0.014	0.144 ± 0.046
HD 23990	17907	95	B9.5V	7.16 ± 0.51	…	…	…	…	…	…	…	…
V766 Tau	18033	100	B9pSi	6.48 ± 0.55	6.310	0.363 ± 0.194	-0.062 ± 0.012	-0.479 ± 0.013	-0.146 ± 0.005	-0.538 ± 0.019	0.083 ± 0.015	0.272 ± 0.048
HD 23662	18067	97	B8V	5.2 ± 0.48	…	…	-0.080	-0.240	-0.080	-0.240	0.000	0.000
HD 24456	18190	98	B9.5V	7.2 ± 0.37	…	…	…	…	…	…	…	…
HD 26323	19466	82	A2V	6.72 ± 0.34	…	…	…	…	…	…	…	…
HD 26676	19720	73	B8Vn	4.87 ± 0.77	6.225 ± 0.084	-0.362 ± 0.379	0.048 ± 0.004	-0.335 ± 0.014	-0.127 ± 0.004	-0.460 ± 0.017	0.175 ± 0.006	0.574 ± 0.020
μ Tau	19860	96	B3IV	7.16 ± 0.34	4.280 ± 0.010	-1.453 ± 0.104	-0.060 ± 0.009	-0.522 ± 0.017	-0.160 ± 0.006	-0.594 ± 0.023	0.100 ± 0.013	0.327 ± 0.041
HR 1328	20063	100	B9V	5.06 ± 0.8	6.210	-0.307 ± 0.359	-0.070 ± 0.007	-0.315 ± 0.011	-0.100 ± 0.003	-0.338 ± 0.014	0.030 ± 0.009	0.099 ± 0.028
53 Tau	20171	97	B9Vsp	12.08 ± 0.36	5.350	0.759 ± 0.066	-0.092 ± 0.019	-0.274 ± 0.015	-0.092 ± 0.019	-0.274 ± 0.015	0.000	0.000
HD 27528	20229	96	A0Vn	5.79 ± 0.41	6.800	0.609 ± 0.157	-0.030	…	…	…	…	…
d Per	20354	100	B4IV	6.43 ± 0.28	4.849 ± 0.010	-1.106 ± 0.097	-0.027 ± 0.010	-0.520 ± 0.012	-0.166 ± 0.004	-0.619 ± 0.017	0.139 ± 0.013	0.454 ± 0.041
HD 27707	20424	96		6.44 ± 0.33	…	…	…	…	…	…	…	…
HR 1415	20884	94	B5V	8.52 ± 0.35	5.545 ± 0.109	0.192 ± 0.138	-0.102 ± 0.004	-0.543 ± 0.005	-0.156 ± 0.002	-0.580 ± 0.007	0.054 ± 0.005	0.176 ± 0.016
HD 28715	21135	100		6.32 ± 0.54	…	…	…	…	…	…	…	…
HD 28796	21177	100		5.04 ± 0.55	…	…	…	…	…	…	…	…
DZ Eri	21192	97	B9IIIpHg	6.86 ± 0.35	5.799 ± 0.020	-0.020 ± 0.109	-0.144 ± 0.011	-0.548 ± 0.016	-0.149 ± 0.005	-0.550 ± 0.022	0.005 ± 0.014	0.017 ± 0.047
HD 29554	21640	86		6.33 ± 0.49	…	…	…	…	…	…	…	…
HD 286987	21973	81	B8	6.01 ± 0.74	…	…	…	…	…	…	…	…
HD 29866	22034	97	B8V	5.28 ± 0.5	6.064 ± 0.023	-0.333 ± 0.207	0.057 ± 0.018	-0.293 ± 0.016	-0.118 ± 0.006	-0.420 ± 0.025	0.177 ± 0.023	0.578 ± 0.074
μ Eri	22109	73	B4IV	6.25 ± 0.19	4.012 ± 0.008	-2.009 ± 0.066	-0.149 ± 0.005	-0.573 ± 0.011	-0.155 ± 0.004	-0.576 ± 0.014	0.006 ± 0.007	0.019 ± 0.022
HD 30122	22128	100	B5III	4.71 ± 0.51	…	…	0.065 ± 0.005	-0.450 ± 0.000	-0.165 ± 0.004	-0.614 ± 0.013	0.230 ± 0.007	0.750 ± 0.022
HD 30409	22415	100	B9V	3.95 ± 0.29	8.310	1.291 ± 0.158	0.070	-0.050	-0.050 ± 0.005	-0.136 ± 0.017	0.120 ± 0.014	0.396 ± 0.046
HD 31799	23130	98		5.51 ± 0.3	…	…	…	…	…	…	…	…
HD 32884	23745	90		5.32 ± 0.76	…	…	…	…	…	…	…	…
η Aur	23767	99	B3V	13.4 ± 0.2	3.172 ± 0.008	-1.193 ± 0.034	-0.178 ± 0.009	-0.669 ± 0.005	-0.180 ± 0.003	-0.669 ± 0.011	0.001 ± 0.012	0.004 ± 0.038
17 Aur	24740	80	B9.5V	7.05 ± 0.61	6.143 ± 0.013	0.368 ± 0.193	-0.059 ± 0.001	-0.136 ± 0.087	-0.059 ± 0.001	-0.136 ± 0.087	0.000	0.000
15 Cam	24836	99	B5V	3.91 ± 0.7	6.120 ± 0.000	-0.967 ± 0.400	-0.024 ± 0.006	-0.479 ± 0.001	-0.154 ± 0.001	-0.571 ± 0.005	0.130 ± 0.007	0.423 ± 0.023
HD 35034	25157	58	B8V	3.38 ± 0.32	8.020	0.647 ± 0.210	0.030	-0.340	-0.125 ± 0.003	-0.451 ± 0.015	0.155 ± 0.012	0.506 ± 0.040
115 Tau	25499	97	B5V	5.94 ± 0.34	5.416 ± 0.008	-0.727 ± 0.123	-0.100 ± 0.001	-0.540 ± 0.000	-0.156 ± 0.003	-0.578 ± 0.012	0.056 ± 0.003	0.181 ± 0.011
116 Tau	25555	62	B9.5Vn	7.69 ± 0.33	…	…	0.010	-0.050	-0.033 ± 0.005	-0.077 ± 0.017	0.043 ± 0.013	0.142 ± 0.044
HD 35785	25561	99		4.64 ± 0.4	…	…	…	…	…	…	…	…
HD 35945	25657	97		5.8 ± 0.69	7.650	1.438 ± 0.268	0.020	-0.120	-0.062 ± 0.004	-0.180 ± 0.016	0.083 ± 0.013	0.273 ± 0.043
118 Tau	25695	84	B8V	7.67 ± 0.73	5.470	-0.121 ± 0.198	-0.045 ± 0.005	-0.174 ± 0.035	-0.064 ± 0.012	-0.187 ± 0.044	0.019 ± 0.013	0.062 ± 0.043
HD 36453	26034	100	B9V	4.07 ± 0.37	6.607 ± 0.033	-0.350 ± 0.207	-0.040 ± 0.028	-0.190	-0.070 ± 0.007	-0.211 ± 0.028	0.028 ± 0.035	0.093 ± 0.113
125 Tau	26640	94	B3IV	7.63 ± 0.33	5.168 ± 0.008	-0.421 ± 0.095	-0.152 ± 0.002	-0.689 ± 0.003	-0.193 ± 0.001	-0.718 ± 0.004	0.041 ± 0.003	0.134 ± 0.009

Table 6 continued

Table 6 *(continued)*

Name	HIP	Prob.	SpT	ϖ	V	M_V	$B-V$	$U-B$	$(B-V)_0$	$(U-B)_0$	$E(B-V)$	A_V
		(%)		(mas)	(mag)	(mag)	(mag)	(mag)	(mag)	(mag)	(mag)	(mag)
HD 38670	27421	87	B9Vn	5.97 ± 0.73	6.070	-0.058 ± 0.273	-0.091 ± 0.009	-0.389 ± 0.025	-0.115 ± 0.007	-0.408 ± 0.032	0.025 ± 0.013	0.081 ± 0.042
HD 39114	27723	100	B9.5IV	4.72 ± 1.04	...	...	...	...	...	...	...	...
HD 39285	27746	93		4.8 ± 1.04	...	...	...	...	...	...	...	...
HD 39773	27962	62	A0III	4.18 ± 0.57	6.800	-0.124 ± 0.307	0.000	-0.360	-0.125 ± 0.003	-0.450 ± 0.015	0.125 ± 0.012	0.410 ± 0.040
nu Ori	29038	100	B3IV	6.32 ± 0.33	4.417 ± 0.007	-1.583 ± 0.113	-0.161 ± 0.013	-0.656 ± 0.022	-0.179 ± 0.008	-0.668 ± 0.030	0.019 ± 0.018	0.061 ± 0.057
HD 44172	30180	95	B8	3.05 ± 0.66	7.340 ± 0.000	-0.294 ± 0.507	-0.100 ± 0.000	-0.511 ± 0.010	-0.147 ± 0.004	-0.543 ± 0.015	0.047 ± 0.012	0.152 ± 0.040
HR 2395	31278	98	B5Vn	5.89 ± 0.24	5.092 ± 0.004	-1.060 ± 0.089	-0.145 ± 0.008	-0.559 ± 0.006	-0.152 ± 0.003	-0.562 ± 0.010	0.007 ± 0.010	0.022 ± 0.033

a. Shell star

REFERENCES

Abt, H. A., Levato, H., & Grosso, M. 2002, ApJ, 573, 359
Aigrain, S., Parviainen, H., & Pope, B. J. S. 2016, MNRAS, 459, 2408
Akeson, R. L., Chen, X., Ciardi, D., et al. 2013, PASP, 125, 989
Anderson, E., & Francis, C. 2012, Astronomy Letters, 38, 331
Angus, R., Aigrain, S., Foreman-Mackey, D., & McQuillan, A. 2015, MNRAS, 450, 1787
Avvakumova, E. A., Malkov, O. Y., & Kniazev, A. Y. 2013, Astronomische Nachrichten, 334, 860
Barnes, J. W., van Eyken, J. C., Jackson, B. K., Ciardi, D. R., & Fortney, J. J. 2013, ApJ, 774, 53
Barnes, S. A. 2007, ApJ, 669, 1167
Barrado y Navascués, D., Stauffer, J. R., & Jayawardhana, R. 2004, ApJ, 614, 386
Bell, C. P. M., Mamajek, E. E., & Naylor, T. 2015, MNRAS, 454, 593
Bessell, M. S. 1990, PASP, 102, 1181
Blaauw, A. 1956, ApJ, 123, 408
Bouvier, J., Barrado, D., Moraux, E., et al. 2017, ArXiv e-prints, arXiv:1712.06525
Bowler, B. P. 2016, PASP, 128, 102001
Boyajian, T. S., von Braun, K., van Belle, G., et al. 2012, ApJ, 757, 112
Brandt, T. D., & Huang, C. X. 2015, ApJ, 807, 24
Bressan, A., Marigo, P., Girardi, L., et al. 2012, MNRAS, 427, 127
Brucalassi, A., Pasquini, L., Saglia, R., et al. 2014, A&A, 561, L9
—. 2016, A&A, 592, L1
Brucalassi, A., Koppenhoefer, J., Saglia, R., et al. 2017, A&A, 603, A85
Buchhave, L. A., Latham, D. W., Johansen, A., et al. 2012, Nature, 486, 375
Buchhave, L. A., Bizzarro, M., Latham, D. W., et al. 2014, Nature, 509, 593
Caffau, E., Ludwig, H.-G., Steffen, M., Freytag, B., & Bonifacio, P. 2011, SoPh, 268, 255
Cardelli, J. A., Clayton, G. C., & Mathis, J. S. 1989, ApJ, 345, 245
Castelli, F., & Kurucz, R. L. 2004, ArXiv Astrophysics e-prints, astro-ph/0405087
Chambers, K. C., Magnier, E. A., Metcalfe, N., et al. 2016, ArXiv e-prints, arXiv:1612.05560
Chen, H., & Rogers, L. A. 2016, ApJ, 831, 180
Chen, J., & Kipping, D. 2017a, ApJ, 834, 17
—. 2017b, Forecaster: Mass and radii of planets predictor, Astrophysics Source Code Library, , , ascl:1701.007
Chen, Y., Girardi, L., Bressan, A., et al. 2014, MNRAS, 444, 2525
Choi, J., Dotter, A., Conroy, C., et al. 2016, ApJ, 823, 102
Chubak, C., Marcy, G., Fischer, D. A., et al. 2012, ArXiv e-prints, arXiv:1207.6212
Ciardi, D. R., Beichman, C. A., Horch, E. P., & Howell, S. B. 2015a, ApJ, 805, 16
Ciardi, D. R., van Eyken, J. C., Barnes, J. W., et al. 2015b, ApJ, 809, 42
Ciardi, D. R., Crossfield, I. J. M., Feinstein, A. D., et al. 2017, ArXiv e-prints, arXiv:1709.10398
Claret, A., Hauschildt, P. H., & Witte, S. 2012, A&A, 546, A14
Cochran, W. D., Hatzes, A. P., & Paulson, D. B. 2002, AJ, 124, 565
Cram, L. E., & Mullan, D. J. 1979, ApJ, 234, 579
Crawford, D. L. 1963, ApJ, 137, 523
—. 1978, AJ, 83, 48
Cumming, A., Butler, R. P., Marcy, G. W., et al. 2008, PASP, 120, 531
Cutri, R. M., & et al. 2013, VizieR Online Data Catalog, 2328
Cutri, R. M., Skrutskie, M. F., van Dyk, S., et al. 2003, 2MASS All Sky Catalog of point sources.
David, T. J., & Hillenbrand, L. A. 2015, ApJ, 804, 146
David, T. J., Hillenbrand, L. A., Petigura, E. A., et al. 2016a, Nature, 534, 658
David, T. J., Conroy, K. E., Hillenbrand, L. A., et al. 2016b, AJ, 151, 112
de Zeeuw, P. T., Hoogerwerf, R., de Bruijne, J. H. J., Brown, A. G. A., & Blaauw, A. 1999, AJ, 117, 354
de Zeeuw, T., & Brand, J. 1985, in Astrophysics and Space Science Library, Vol. 120, Birth and Evolution of Massive Stars and Stellar Groups, ed. W. Boland & H. van Woerden, 95–101
Dobbie, P. D., Lodieu, N., & Sharp, R. G. 2010, MNRAS, 409, 1002
Donati, J. F., Moutou, C., Malo, L., et al. 2016, Nature, 534, 662

Douglas, S. T., Agüeros, M. A., Covey, K. R., et al. 2016, ApJ, 822, 47
Findeisen, K., & Hillenbrand, L. 2010, AJ, 139, 1338
Findeisen, K., Hillenbrand, L., & Soderblom, D. 2011, AJ, 142, 23
Fischer, D. A., & Valenti, J. 2005, ApJ, 622, 1102
Flewelling, H. A., Magnier, E. A., Chambers, K. C., et al. 2016, ArXiv e-prints, arXiv:1612.05243
Foreman-Mackey, D., Hogg, D. W., Lang, D., & Goodman, J. 2013, PASP, 125, 306
Fulton, B. J., Petigura, E. A., Blunt, S., & Sinukoff, E. 2018, ArXiv e-prints, arXiv:1801.01947
Fulton, B. J., Petigura, E. A., Howard, A. W., et al. 2017, AJ, 154, 109
Gaia Collaboration, Prusti, T., de Bruijne, J. H. J., et al. 2016a, A&A, 595, A1
Gaia Collaboration, Brown, A. G. A., Vallenari, A., et al. 2016b, A&A, 595, A2
Gaidos, E., Mann, A. W., Rizzuto, A., et al. 2017, MNRAS, 464, 850
Gilliland, R. L., Brown, T. M., Guhathakurta, P., et al. 2000, ApJL, 545, L47
Girardi, L., Groenewegen, M. A. T., Hatziminaoglou, E., & da Costa, L. 2005, A&A, 436, 895
Gontcharov, G. A. 2006, Astronomy Letters, 32, 759
Hartmann, L., Stauffer, J. R., Kenyon, S. J., & Jones, B. F. 1991, AJ, 101, 1050
Henden, A. A., Templeton, M., Terrell, D., et al. 2016, VizieR Online Data Catalog, 2336
Hernán-Obispo, M., Gálvez-Ortiz, M. C., Anglada-Escudé, G., et al. 2010, A&A, 512, A45
Hernán-Obispo, M., Tuomi, M., Gálvez-Ortiz, M. C., et al. 2015, A&A, 576, A66
Hillenbrand, L., Isaacson, H., Marcy, G., et al. 2015, in Cambridge Workshop on Cool Stars, Stellar Systems, and the Sun, Vol. 18, 18th Cambridge Workshop on Cool Stars, Stellar Systems, and the Sun, ed. G. T. van Belle & H. C. Harris, 759–766
Howard, A. W., Marcy, G. W., Bryson, S. T., et al. 2012, ApJS, 201, 15
Howarth, I. D. 2016, MNRAS, 457, 3769
Howell, S. B., Rowe, J. F., Bryson, S. T., et al. 2012, ApJ, 746, 123
Howell, S. B., Sobeck, C., Haas, M., et al. 2014, PASP, 126, 398
Huber, D., Bryson, S. T., Haas, M. R., et al. 2016, ApJS, 224, 2
Janes, K., & Kim, J.-H. 2009, in IAU Symposium, Vol. 253, Transiting Planets, ed. F. Pont, D. Sasselov, & M. J. Holman, 548–551
Johns-Krull, C. M., McLane, J. N., Prato, L., et al. 2016a, ApJ, 826, 206
Johns-Krull, C. M., Prato, L., McLane, J. N., et al. 2016b, ApJ, 830, 15
Kamai, B. L., Vrba, F. J., Stauffer, J. R., & Stassun, K. G. 2014, AJ, 148, 30
Kolbl, R., Marcy, G. W., Isaacson, H., & Howard, A. W. 2015, AJ, 149, 18
Kovács, G., Zucker, S., & Mazeh, T. 2002, A&A, 391, 369
Kraus, A. L., Shkolnik, E. L., Allers, K. N., & Liu, M. C. 2014, AJ, 147, 146
Kreidberg, L. 2015, PASP, 127, 1161
Kurucz, R. L. 1992, in IAU Symposium, Vol. 149, The Stellar Populations of Galaxies, ed. B. Barbuy & A. Renzini, 225
Libralato, M., Nardiello, D., Bedin, L. R., et al. 2016, MNRAS, 463, 1780
Livingston, J. H., Dai, F., Hirano, T., et al. 2017, ArXiv e-prints, arXiv:1710.07203
Lomb, N. R. 1976, Ap&SS, 39, 447
Lopez, E. D., & Fortney, J. J. 2013, ApJ, 776, 2
López-Morales, M., & Ribas, I. 2005, ApJ, 631, 1120
Lovis, C., & Mayor, M. 2007, A&A, 472, 657
Luhman, K. L., Mamajek, E. E., Allen, P. R., & Cruz, K. L. 2009, ApJ, 703, 399
Madsen, S., Dravins, D., & Lindegren, L. 2002, A&A, 381, 446
Maíz Apellániz, J. 2006, AJ, 131, 1184
Malavolta, L., Nascimbeni, V., Piotto, G., et al. 2016, A&A, 588, A118
Mamajek, E. E. 2005, ApJ, 634, 1385
Mamajek, E. E., & Bell, C. P. M. 2014, MNRAS, 445, 2169
Mamajek, E. E., & Hillenbrand, L. A. 2008, ApJ, 687, 1264
Mandel, K., & Agol, E. 2002, ApJL, 580, L171
Mann, A. W., Feiden, G. A., Gaidos, E., Boyajian, T., & von Braun, K. 2015, ApJ, 804, 64
Mann, A. W., Newton, E. R., Rizzuto, A. C., et al. 2016a, AJ, 152, 61

Mann, A. W., Gaidos, E., Mace, G. N., et al. 2016b, ApJ, 818, 46
Mann, A. W., Vanderburg, A., Rizzuto, A. C., et al. 2017a, ArXiv e-prints, arXiv:1709.10328
Mann, A. W., Gaidos, E., Vanderburg, A., et al. 2017b, AJ, 153, 64
Martin, D. C., Fanson, J., Schiminovich, D., et al. 2005, ApJL, 619, L1
Masuda, K., & Winn, J. N. 2017, AJ, 153, 187
Mayor, M., Udry, S., Naef, D., et al. 2004, A&A, 415, 391
Meibom, S., Torres, G., Fressin, F., et al. 2013, Nature, 499, 55
Mentuch, E., Brandeker, A., van Kerkwijk, M. H., Jayawardhana, R., & Hauschildt, P. H. 2008, ApJ, 689, 1127
Mermilliod, J. C. 1981, A&A, 97, 235
—. 2006, VizieR Online Data Catalog, 2168
Mermilliod, J.-C., Weis, E. W., Duquennoy, A., & Mayor, M. 1990, A&A, 235, 114
Meynet, G., Mermilliod, J.-C., & Maeder, A. 1993, A&AS, 98, 477
Morton, T. D. 2015, VESPA: False positive probabilities calculator, Astrophysics Source Code Library, , , ascl:1503.011
Obermeier, C., Henning, T., Schlieder, J. E., et al. 2016, AJ, 152, 223
Onitsuka, M., Fukui, A., Narita, N., et al. 2017, PASJ, 69, L2
Owen, J. E., & Wu, Y. 2013, ApJ, 775, 105
Paunzen, E. 2015, A&A, 580, A23
Pecaut, M. J., & Mamajek, E. E. 2013, ApJS, 208, 9
—. 2016, MNRAS, 461, 794
Pepper, J., Gillen, E., Parviainen, H., et al. 2017, AJ, 153, 177
Perryman, M. A. C., Brown, A. G. A., Lebreton, Y., et al. 1998, A&A, 331, 81
Petigura, E. A., Howard, A. W., Marcy, G. W., et al. 2017, AJ, 154, 107
Petrie, R. M. 1958, MNRAS, 118, 80
Plavchan, P., Latham, D., Gaudi, S., et al. 2015, ArXiv e-prints, arXiv:1503.01770
Prosser, C. F. 1992, AJ, 103, 488
Quinn, S. N., White, R. J., Latham, D. W., et al. 2012, ApJL, 756, L33
—. 2014, ApJ, 787, 27
Raetz, S., Schmidt, T. O. B., Czesla, S., et al. 2016, MNRAS, 460, 2834
Randich, S., Pallavicini, R., Meola, G., Stauffer, J. R., & Balachandran, S. C. 2001, A&A, 372, 862
Rasmuson, N. H. 1921, Meddelanden fran Lunds Astronomiska Observatorium Serie II, 26, 3
Rebull, L. M., Stauffer, J. R., Hillenbrand, L. A., et al. 2017, ApJ, 839, 92
Rebull, L. M., Stauffer, J. R., Bouvier, J., et al. 2016, AJ, 152, 113
Rizzuto, A. C., Mann, A. W., Vanderburg, A., Kraus, A. L., & Covey, K. R. 2017, AJ, 154, 224
Robichon, N., Arenou, F., Turon, C., Lebreton, Y., & Mermilliod, J.-C. 1998, Highlights of Astronomy, 11, 579
Rodriguez, D. R., Bessell, M. S., Zuckerman, B., & Kastner, J. H. 2011, ApJ, 727, 62
Rodriguez, D. R., Zuckerman, B., Kastner, J. H., et al. 2013, ApJ, 774, 101
Sato, B., Izumiura, H., Toyota, E., et al. 2007, ApJ, 661, 527
Scargle, J. D. 1982, ApJ, 263, 835
Seager, S., & Mallén-Ornelas, G. 2003, ApJ, 585, 1038
Shkolnik, E. L., Liu, M. C., Reid, I. N., Dupuy, T., & Weinberger, A. J. 2011, ApJ, 727, 6
Shobbrook, R. R. 1983, MNRAS, 205, 1215
Skiff, B. A. 2014, VizieR Online Data Catalog, 1
Soderblom, D. R., Hillenbrand, L. A., Jeffries, R. D., Mamajek, E. E., & Naylor, T. 2014, Protostars and Planets VI, 219
Soderblom, D. R., Jones, B. F., Balachandran, S., et al. 1993, AJ, 106, 1059
Stauffer, J. 1982, PASP, 94, 678
Stauffer, J., Rebull, L., Bouvier, J., et al. 2016, AJ, 152, 115
Stauffer, J. R., & Hartmann, L. W. 1987, ApJ, 318, 337
Stauffer, J. R., Hartmann, L. W., & Jones, B. F. 1989, ApJ, 346, 160
Stauffer, J. R., Barrado y Navascués, D., Bouvier, J., et al. 1999, ApJ, 527, 219
Upgren, A. R., Weis, E. W., & Deluca, E. E. 1979, AJ, 84, 1586
van Eyken, J. C., Ciardi, D. R., von Braun, K., et al. 2012, ApJ, 755, 42
van Leeuwen, F. 2007, A&A, 474, 653
van Saders, J. L., & Gaudi, B. S. 2011, ApJ, 729, 63
Vanderburg, A., & Johnson, J. A. 2014, PASP, 126, 948

Vanderburg, A., Latham, D. W., Buchhave, L. A., et al. 2016, ApJS, 222, 14
Vazan, A., Ormel, C. W., & Dominik, C. 2017, ArXiv e-prints, arXiv:1712.06158
Ventura, P., Zeppieri, A., Mazzitelli, I., & D'Antona, F. 1998, A&A, 334, 953
Vogt, S. S., Allen, S. L., Bigelow, B. C., et al. 1994, in Proc. SPIE, Vol. 2198, Instrumentation in Astronomy VIII, ed. D. L. Crawford & E. R. Craine, 362
Walter, F. M., & Boyd, W. T. 1991, ApJ, 370, 318
Walter, F. M., Brown, A., Mathieu, R. D., Myers, P. C., & Vrba, F. J. 1988, AJ, 96, 297
Weis, E. W. 1981, PASP, 93, 437
Weldrake, D. T. F., Sackett, P. D., & Bridges, T. J. 2008, ApJ, 674, 1117
Weldrake, D. T. F., Sackett, P. D., Bridges, T. J., & Freeman, K. C. 2005, ApJ, 620, 1043
Yee, S. W., Petigura, E. A., & von Braun, K. 2017, ApJ, 836, 77
Yu, L., Winn, J. N., Gillon, M., et al. 2015, ApJ, 812, 48
Yu, L., Donati, J.-F., Hébrard, E. M., et al. 2017, MNRAS, 467, 1342
Yuan, H. B., Liu, X. W., & Xiang, M. S. 2013, MNRAS, 430, 2188
Zacharias, N., Finch, C., & Frouard, J. 2017, AJ, 153, 166